Modeling and Simulation of a Novel Membrane Reactor in a Continuous Catalytic Regenerative Naphtha Reformer Accompanied with a Detailed Description of Kinetics

ARTICLE *in* ENERGY & FUELS · JULY 2013

Impact Factor: 2.79 · DOI: 10.1021/ef302057k

6 AUTHORS, INCLUDING:

Davood Iranshahi
Amirkabir University of Technology
50 PUBLICATIONS **391** CITATIONS
SEE PROFILE

Salman Amiri
Allameh Tabatabai University
12 PUBLICATIONS **22** CITATIONS
SEE PROFILE

Mohsen Karimi
Shiraz University
13 PUBLICATIONS **34** CITATIONS
SEE PROFILE

M. R. Rahimpour
Shiraz University
331 PUBLICATIONS **3,022** CITATIONS
SEE PROFILE

energy&fuels

Article

pubs.acs.org/EF

Modeling and Simulation of a Novel Membrane Reactor in a Continuous Catalytic Regenerative Naphtha Reformer Accompanied with a Detailed Description of Kinetics

Davood Iranshahi,[†] Shahram Amiri,[†] Mohsen Karimi,[†] Razieh Rafiei,[†] Mitra Jafari,[†] and Mohammad Reza Rahimpour*[,†,‡]

[†]Department of Chemical Engineering, School of Chemical and Petroleum Engineering, Shiraz University, Shiraz 71345, Iran

[‡]Department of Chemical Engineering and Materials Science, University of California—Davis, 1 Shields Avenue, Davis, California 95616, United States

ABSTRACT: Today, improving the performance of reformers by increasing the octane number of products has received more attention in refineries. In this regard, researchers have been looking for ways of increasing the content of high-octane number products such as aromatics. The present research proposes an alternative configuration for a conventional moving bed naphtha reactor. In this new configuration, the membrane concept is applied in the moving bed reactors to increase the aromatics and hydrogen yields. Most studies on the simulation of continuous catalytic regenerative (CCR) naphtha reactors focused on a one-dimensional mathematical model, while in this work, a two-dimensional mathematical model (in the radial and axial directions) is considered. In the process model, a new reaction network based on 32 pseudocomponents and 84 reactions, as well as a new deactivation model including the most effective parameters, is considered. To verify the efficiency of the conventional configuration model, its results are compared with the industrial data. Results demonstrate that the application of a membrane can increase the aromatics and hydrogen production rates by about 54 and 220 kmol/h, respectively.

1. INTRODUCTION

1.1. Naphtha Reforming. The catalytic reformer plays a very important role in refineries. It provides high value-added reformate for gasoline pool; hydrogen for improving feedstock by hydrogen-consuming hydrotreatment processes; and valuable aromatics such as benzene, toluene, and xylenes for petrochemical uses.[1] The main aim of catalytic naphtha reforming is to change naphthenes and paraffins to aromatics, which have high-octane numbers and can increase the gasoline octane number.[2] In order to improve the performance of this process, a large number of studies have been done. Many researchers have been focused on the kinetics of catalytic naphtha reforming. Since a large number of reactions consisting of hundreds of various components occur in reformers, unfortunately developing a detailed kinetic-based model, which considered all components and reactions, is not easily possible. For this reason, researchers have been tried to model naphtha reactions by considering kinetic lumps taking part in the naphtha reforming reactions.[3] Smith[4] as a pioneer of the researchers presented a model containing paraffins, naphthenes, and aromatics and four main reactions. More detailed kinetic models to describe the reforming process have been reported by Krane et al.,[5] Kmak,[6] Ramage et al.,[7] Jenkins et al.,[8] and Wolff et al.[9] and, in the past decade, by Juarez et al.[10] and Sotelo-Boyas and Froment.[11] The researchers developed different kinetic models of a varying number of lump components. For instance, Hu et al. proposed a simple model of catalytic reforming with 17 lumps involving 17 reactions.[12] Hu and Zhu used a model involving 21 classes of molecules and 51 reactions.[13] Hongjun et al. developed a lumped kinetic model with 27 lumps in order to predict aromatic compositions in more detail.[14]

Recently, catalysts and catalyst deactivation of reforming processes have received more attention. In this regard, studies have been performed by Otal et al.,[15] Gonzalez-Marcos et al.,[16] Pieck et al.,[17] Ren et al.,[18] Carvalho et al.,[19] Borgna et al.,[20] Viswanadham et al.,[21] and Martin et al.[22] to improve the performance of catalysts and process. Other attempts on the naphtha reforming process have been done on the modeling and improving of hydrogen and aromatic yields. Taskar et al.[23] modeled and optimized a semiregenerative catalytic naphtha reformer involving most of its key constitutes. Juarez et al.[24] presented a modeling and simulation of naphtha reforming process. They used an extended version of the kinetic model reported by Krane et al. The other appropriate studies in this field have been performed by Li et al.[25] and Hou et al.[26]

1.2. Process Classification. Generally, the naphtha reforming process based on mode of catalysts regeneration is classified into the semiregenerative, cyclic, and continuous catalytic regenerative processes. The semiregenerative systems typically use three to four beds in series and operate continuously over long periods (typically up to 1 y). As the deposited coke on the catalysts increases, the reformers are shut down to regenerate catalysts. The research octane numbers in the semiregenerative process are in the range of 85−100.[2] The detailed explanation can be found in the previous publication.[27] The cyclic systems typically use five or six fixed catalyst beds

Received: December 12, 2012
Revised: March 14, 2013
Published: March 14, 2013

   dx.doi.org/10.1021/ef302057k | *Energy Fuels* 2013, 27, 4048−4070

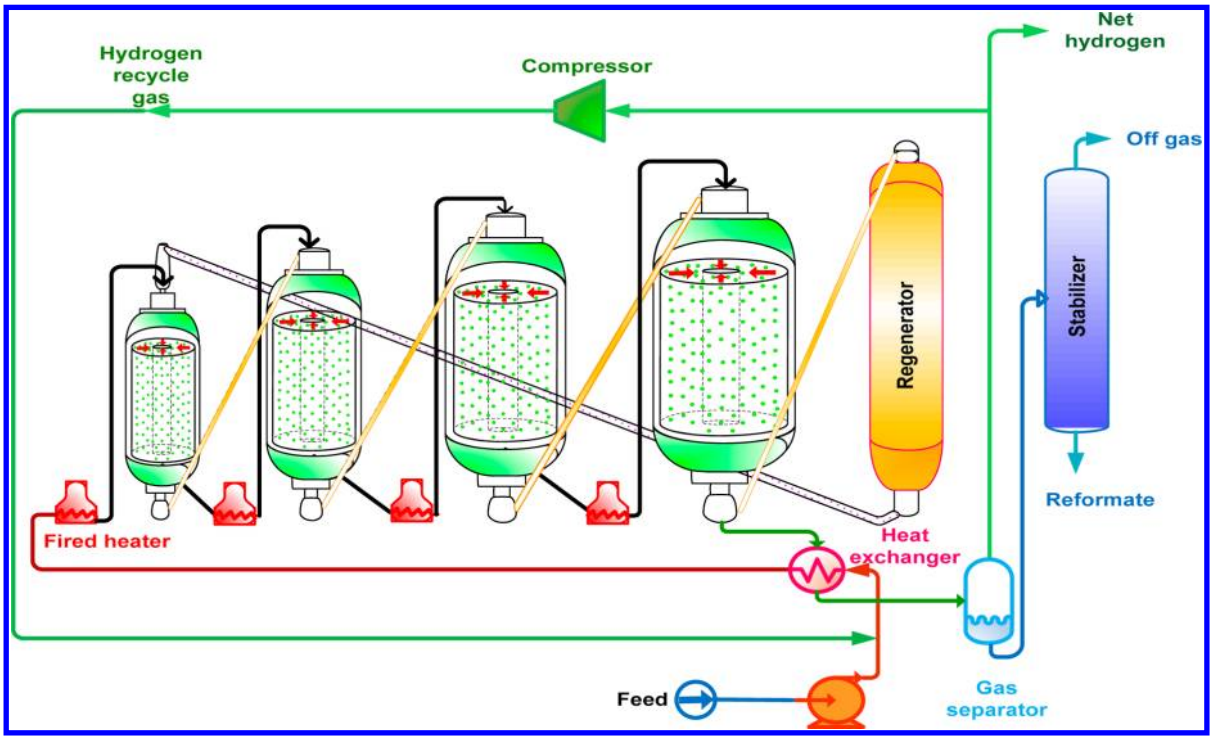

Figure 1. Schematic diagram of the conventional CCR process.

with a swing reactor. Each reactor in a series of reactors can be taken out of operation for regeneration without shutting down the unit. The research octane numbers of this process are around 100.[28] The most modern type of the catalytic reformers is the continuous catalytic regenerative (CCR) reformer, which represents a step change in reforming technology compared to the semiregenerative and cyclic processes. In this unit, the catalyst regenerates continuously in a special regenerator and then is sent to the operating reactors. In this process, higher aromatic content, high hydrogen purity, and catalyst activity can be observed. CCR units operate at ultralow pressure, and their design research octane number is in the range of 95–108.[2,28] Although most grassroots reformers are designed for CCR, a few published works regarding modeling of naphtha reforming process have been done on CCR.[3,14,28−31]

1.3. Membrane Reactor. By removing reactants from product gases, the equilibrium compositions can shift toward the product side. One idea for performing this work is membrane application. The membrane concept is a well-known technology for separation. Separation via membrane is less energy intensive and requires no phase change in the process.[32] The Pd–Ag membrane layer with silver content of 23–25% is extensively utilized for hydrogen purification.[33,34] A number of factors, including low costs, perm selectivity, good mechanical/thermal, and long-term stability are the reasons of successful development of this type of membrane.[35] In the naphtha process, employing this membrane can shift the dehydrogenation reactions toward the aromatic production via extracting hydrogen. Today, as many as 100 membrane plants have been used in the refineries, but still large opportunities to utilize membrane technology in refineries exist.[36] Recently, Rahimpour et al. used Pd–Ag membrane to extract hydrogen from the naphtha reaction regions for enhancement of the octane number of products in the semiregenerative process.[37]

1.4. Hydrogen. Hydrogen has received special attention as an ideal energy carrier because of its fascinating properties, such as being highly efficient and free from pollution.[38] Moreover, hydrogen is a critical feedstock and raw material in petroleum and petrochemical units. Refineries require a large quantity of hydrogen to remove sulfur and nitrogen components and to produce lighter fuels. As the crude oil becomes heavier, more sulfur and nitrogen must be removed and more hydrotreating and hydrocracking processes are needed. Therefore, hydrogen is considered as a critical issue to the world's refineries.[39] In this regard, some attempts have been made to manage hydrogen uses.[40,41] An alternative way is the membrane utilization that can improve the refiner's efficiency via producing more hydrogen.

1.5. Objective. The main goal of this study is to investigate the performance of membrane incorporation in the continuous catalytic regenerative reformers and to evaluate the product contents especially aromatics and hydrogen by comparison with the conventional values. In this work, a two-dimensional mathematical model has been performed to predict the trend of parameters along both radial and axial directions. The process model is accompanied with a new reaction network containing 32 pseudocomponents with 84 reactions and a new deactivation model including both metallic and acidic functions. Additionally, a comparison between the membrane reactor (MR) and conventional reactor (CR) is proposed to show the superiority of this novel configuration.

2. PROCESS DESCRIPTION

2.1. Conventional System. A simple schematic diagram of CCR process is presented in Figure 1. Conventional processes typically use a series of four individual radial-flow reactors and a regeneration system. The regenerated catalysts enter the top of the first reactor and transport through the reactor by gravity flow while it is coked continuously. The catalysts move from the bottom of one reactor to the top of next one and eventually exit from the last reactor, regenerated in the regenerator, and

dx.doi.org/10.1021/ef302057k | Energy Fuels 2013, 27, 4048–4070

then transported back to the first reactor. As shown in Figure 2, while the catalysts move axially inside the reactor, the feed

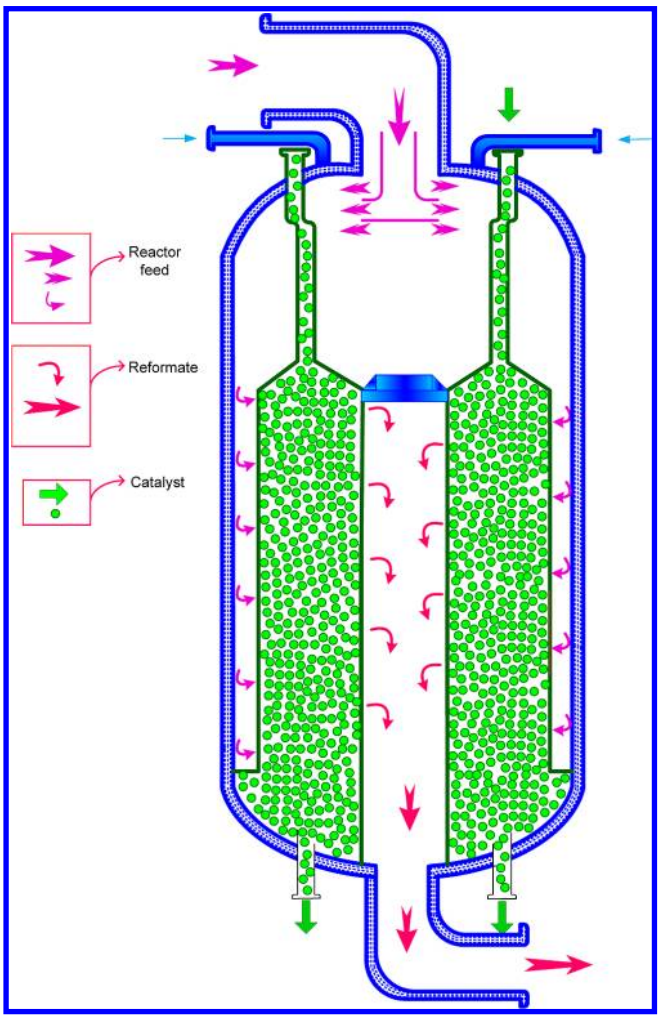

Figure 2. Simple diagram of conventional reactor (CR).

enters the catalyst bed radially. The naphtha feed, after mixing with hydrogen recycle gas stream due to regulation of the inlet ratio of H_2/HC, enters the top of first reactor. It proceeds downward near the shell of the reactor and then goes through the catalyst bed in the radial direction. After passing through the catalyst bed, the obtained stream enters an axial collector and then goes to the next reactor. This procedure is continuous for the other reactors, and eventually, the obtained stream of the fourth reactor is sent to a separator in which hydrogen-rich gas is separated from hydrocarbons. After separation, the obtained liquid is sent to a stabilizer where the off gas is removed from the final reformate. In this process, a highly stable and selective catalyst for continuous regeneration is used. This catalyst is spherically shaped to facilitate catalyst circulation. The gas-lift method is used for catalyst circulation between the reactors and the regenerator. Table 1 shows the specific properties and operating conditions for the conventional configuration.

2.2. Membrane Configuration. As extracting hydrogen can shift the naphtha reactions to produce more aromatics, the membrane layer is applied to the reactors to perform this work. It can be seen in the MR schematic diagram (Figure 3) that the cross-sectional area is divided into some subsections.

Table 1. Specific Properties and Operating Conditions for the Conventional and Membrane Configurations

parameter	numerical value	unit
naphtha feed stock	233637.01	kg/h
H_2/HC mole ratio	2.193	
mole percent of hydrogen in recycle	0.83	
Distillation Fraction of Naphtha Feed		
ASTM D86	naphtha feed (°C)	
IBP	81	
5%	91.2	
10%	93.2	
20%	96.9	
30%	101.1	
40%	105.7	
50%	111.4	
60%	117.6	
70%	124.5	
80%	132.7	
90%	143.1	
95%	150.5	
FBP	159	
Typical Properties of Catalyst		
d_p	1.8	mm
Pt	0.3	wt %
Sn	0.3	wt %
s_a	220	m^2/g
ρ_B	680	kg/m^3
ε	0.36	

Specific Properties and Operating Conditions for the Conventional Configuration

	1st reactor	2nd reactor	3rd reactor	4th reactor
inlet temperature (K)	798	798	798	798
inlet pressure (kPa)	595	550	505	460
inner and outer diameter (m)	1.25, 2.19	1.25, 2.35	1.30, 2.53	1.30, 2.89
length (m)	8.50	10.35	12.1	15.39
catalyst distribution (wt %)	12	18	25	45

Specific Properties and Operating Conditions for the Membrane Configuration

	1st reactor	2nd reactor	3rd reactor	4th reactor
inlet temperature (K)	798	798	798	798
inlet pressure for reaction side (kPa)	595	550	505	460
inlet pressure for sweep side (kPa)	120	120	120	120
inner and outer diameter (m)	1.25, 2.28	1.25, 2.45	1.30, 2.64	1.30, 3.03
length (m)	8.86	10.81	12.63	16.12
NOS (number of subsection)	47	30	24	13
membrane thickness (μm)	10	10	10	10
$R_\theta = \theta_1/(\theta_1 + \theta_2)$	0.85	0.85	0.85	0.85
catalyst distribution (wt %)	12	18	25	45

Each subsection consists of two parts. One is for the naphtha reforming reaction, and the other is for the sweep gas. These parts are separated by a wall which is coated by a Pd−Ag membrane layer. The permeated hydrogen is carried by the sweep gas, which flows radially through the permeation part. The number of subsections is chosen by considering the inverse relation between the number of subsections and H_2/HC molar ratio. By increasing the number of subsections, the area of the membrane layer increases and more hydrogen is permeated and as a consequence, a decrease in the H_2/HC molar ratio appears.

dx.doi.org/10.1021/ef302057k | Energy Fuels 2013, 27, 4048−4070

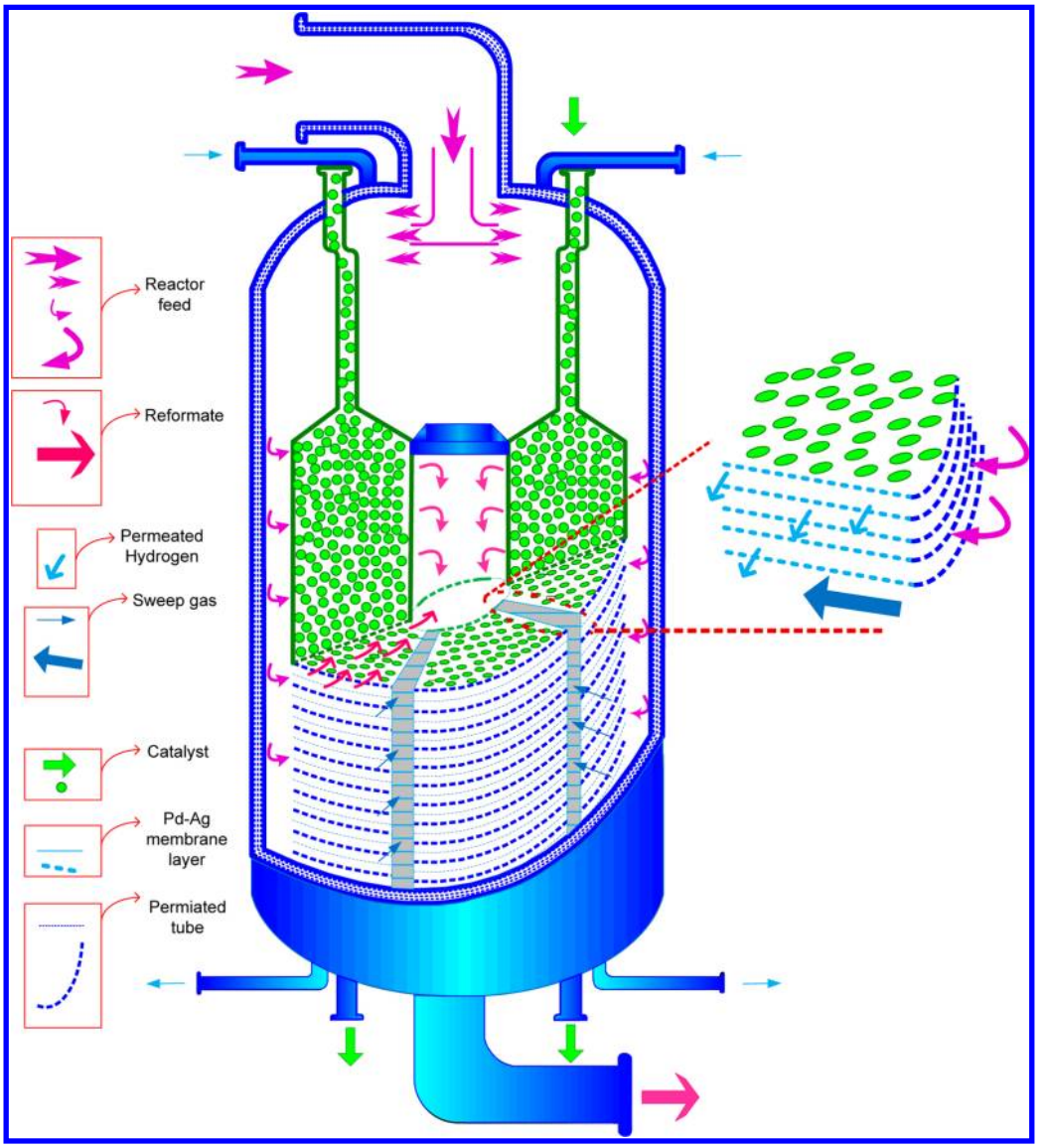

Figure 3. Diagram of membrane reactor (MR).

The H_2/HC molar ratio should not be lower than 2.193 (the inlet H_2/HC ratio of the first reactor) to avoid rapid coking. To reach this goal, the number of subsections is adjusted to 47, 30, 24, and 13 for the first reactor to the fourth one, respectively. In the naphtha reforming, as the feedstock passes through the reactors, the rate of hydrogen production declines; thus, the required subsection decreases from reactor to reactor. In this configuration like the conventional one, catalysts move axially and the feed goes through the catalyst bed in the radial direction. Table 1 shows the specific properties and operating conditions for the new configuration.

3. REACTION SCHEME AND KINETIC EXPRESSIONS

In the reformers, a large number of reactions involving several hundred components take part. As a detailed kinetic-based model considering all components and reactions is infeasible, attempts have been made to reduce the complexity of reactions by considering kinetic lumps taking part in reforming reactions.[3] An effective kinetic model must represent all major reactions in the reforming process. Among the presented kinetic models, one of the appropriate models is that reported by Padmavathi et al.[42] The present kinetic model is an extension of Padmathavi's model. Figure 4 shows the proposed reaction scheme. As can be seen, all major reactions are considered in the model. The eight-carbon aromatics are subdivided into ethyl benzene, *para*-xylene, *ortho*-xylene, and *meta*-xylene which undergo the isomerization reactions, as well as transalkylation reactions. The reactions which added to Padmavathi's kinetic model are marked in the reaction tables. The reactions have been categorized as dehydrogenation, dehydrocyclization, isomerization, transalkylation, hydrocracking, and hydrodealkylation, and their rates and constants are tabulated in Tables 2−7, respectively. Dehydrogenation reaction is one of the major reforming reactions which, due to their high reaction rate, occur mostly in the first reactor to transport naphthenes to aromatics. It is a very fast and highly endothermic reaction and causes a sharp temperature decrease in the first reactor. It is promoted by the metallic function of catalysts and is favored at high temperature and low pressure. The next type of reactions is dehydrocyclization that introduced as the most critical reaction in the reforming process. Like dehydrogenation, dehydrocyclization is favored at

dx.doi.org/10.1021/ef302057k | *Energy Fuels* 2013, 27, 4048−4070

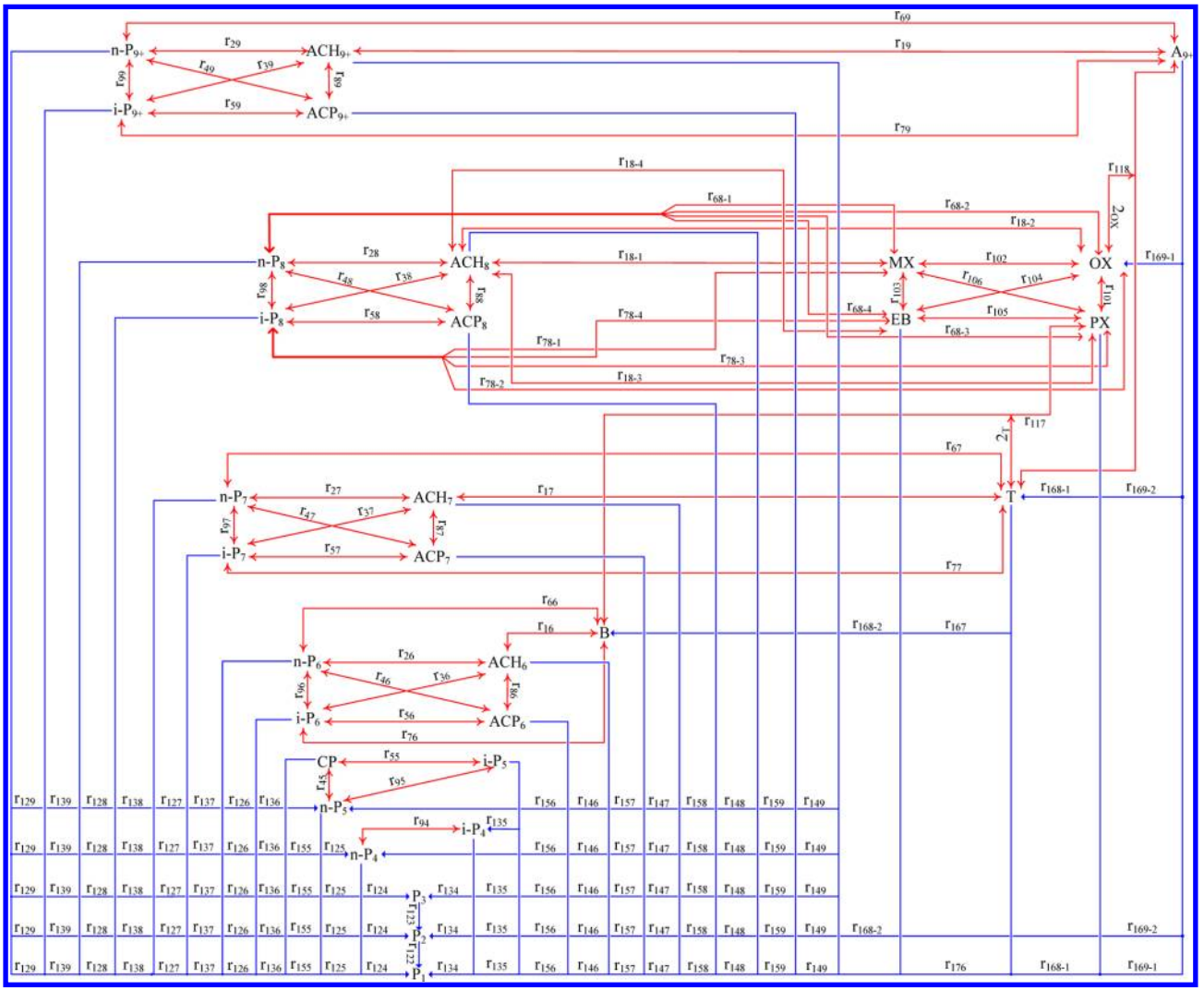

Figure 4. Proposed reactions network for catalytic reforming of naphtha.

Table 2. Rate Constants and the Heat of Dehydrogenation Reactions

$$\mathrm{ACH}_n \leftrightarrow A_n + 3\mathrm{H}_2 \quad r_{1n} = k_{1n}\left(P_{\mathrm{ACH}n} - \frac{P_{A_n}P_{\mathrm{H}_2}{}^3}{K_{1n}}\right) \quad k_{1n} = \underset{(\mathrm{kmol}/(\mathrm{kg_{cat}\ h\ kPa}))}{\exp\left(a - \frac{E}{RT}\right)} \quad K_{1n} = \underset{(\mathrm{kPa})^3}{\exp\left(A - \frac{B}{T}\right)} \qquad (1)$$

	ΔH (kJ/mol H_2)	a	E/R	A	B
C_6	68.73	18.75	19.50	59.90	24.80×10^3
C_7	208.47	20.70	19.50	60.23	25.08×10^3
C_8					
for A_n = MX[a]	64.50	17.89	19.50	60.37	23.27×10^3
for A_n = OX[a]	65.10	19.15	19.50	60.32	23.49×10^3
for A_n = PX[a]	64.74	18.66	19.50	60.13	23.36×10^3
for A_n = EB[a]	68.70	18.71	19.50	60.40	24.78×10^3
C_9^+	66.05	20.38	19.50	61.05	21.33×10^3

[a]Reactions added into the Padmavathi et al.[42] model.

high temperature and low pressure. Although, the rate of dehydrocyclization is comparatively slow, the conversion of paraffins to aromatics causes a noticeable increase in aromatic contents. Dehydrocyclization reaction is promoted by the metallic and acidic sites of catalyst.

The isomerization of paraffins, naphthenes, and aromatics have been considered in the present model. Isomerization reactions are moderately rapid and catalyzed by acid sites. The isomerization of *n*-paraffins to *i*-paraffins is highly desirable reaction because the product of this reaction (iso-paraffins) has a high octane number. The isomerization of alkylcyclopentane to alkylcyclohexane is similar to paraffin isomerization and, due to dehydrogenation of ACH to aromatics, is considered as a desirable reaction. For the eight-carbon aromatics, the

dx.doi.org/10.1021/ef302057k | *Energy Fuels* 2013, 27, 4048−4070

Table 3. Rate Constants and the Heat of (A) Paraffin Dehydrocyclization to Naphthene Reactions and (B) Paraffin Dehydrocyclization to Aromatic Reactions

A

$$ACH_n + H_2 \leftrightarrow NP_n \quad r_{2n} = k_{2n}\left(P_{ACHn}P_{H2} - \frac{P_{NPn}}{K_{2n}}\right) \quad k_{2n} = \exp\left(a - \frac{E}{RT}\right)_{(kmol/(kg_{cat}\ h\ kPa^2))} \quad K_{2n} = \exp\left(A - \frac{B}{T}\right)_{(1/kPa)} \quad (2)$$

	ΔH (kJ/mol)	a	E/R	A	B
C_6	−43.64	24.37	33.11	−9.12	-5.24×10^3
C_7	−32.85	29.10	33.11	−8.95	-3.95×10^3
C_8	−32.55	27.81	33.11	−8.34	-3.91×10^3
C_9^+	−28.00	29.76	33.11	−8.12	-3.37×10^3

$$ACH_n + H_2 \leftrightarrow IP_n \quad r_{3n} = k_{3n}\left(P_{ACHn}P_{H2} - \frac{P_{IPn}}{K_{3n}}\right) \quad k_{3n} = \exp\left(a - \frac{E}{RT}\right)_{(kmol/(kg_{cat}\ h\ kPa^2))} \quad K_{3n} = \exp\left(A - \frac{B}{T}\right)_{(1/kPa)} \quad (3)$$

	ΔH (kJ/mol)	a	E/R	A	B
C_6	−52.00	26.36	33.11	−14.35	-6.25×10^3
C_7	−39.30	25.75	33.11	−13.65	-4.73×10^3
C_8	−49.40	29.00	33.11	−13.17	-5.94×10^3
C_9^+	−49.00	29.76	33.11	−12.39	-5.89×10^3

$$NP_n \leftrightarrow ACP_n + H_2 \quad r_{4n} = k_{4n}\left(P_{NPn} - \frac{P_{ACPn}P_{H2}}{K_{4n}}\right) \quad k_{4n} = \exp\left(a - \frac{E}{RT}\right)_{(kmol/(kg_{cat}\ h\ kPa))} \quad K_{4n} = \exp\left(A - \frac{B}{T}\right)_{(kPa)} \quad (4)$$

	ΔH (kJ/mol)	a	E/R	A	B
C_5[a]	69.73	30.75	33.11	14.39	8.38×10^3
C_6	60.74	31.94	33.11	14.77	7.31×10^3
C_7	60.75	33.43	33.11	14.63	7.31×10^3
C_8	61.75	31.31	33.11	15.98	7.43×10^3
C_9^+	59.00	32.96	33.11	15.21	7.09×10^3

$$IP_n \leftrightarrow ACP_n + H_2 \quad r_{5n} = k_{5n}\left(P_{IPn} - \frac{P_{ACPn}P_{H2}}{K_{5n}}\right) \quad k_{5n} = \exp\left(a - \frac{E}{RT}\right)_{(kmol/(kg_{cat}\ h\ kPa))} \quad K_{5n} = \exp\left(A - \frac{B}{T}\right)_{(kPa)} \quad (5)$$

	ΔH (kJ/mol)	a	E/R	A	B
C_5[a]	76.67	29.83	33.11	16.18	9.22×10^3
C_6	70.60	30.87	33.11	16.03	8.50×10^3
C_7	67.20	32.95	33.11	15.47	8.08×10^3
C_8	78.60	34.19	33.11	16.37	9.45×10^3
C_{9+}	80.00	32.96	33.11	16.02	9.62×10^3

B

$$NP_n \leftrightarrow A_n + 4H_2 \quad r_{6n} = k_{6n}\left(P_{NPn} - \frac{P_{An}P_{H2}^4}{K_{6n}}\right) \quad k_{6n} = \exp\left(a - \frac{E}{RT}\right)_{(kmol/(kg_{cat}\ h\ kPa))} \quad K_{6n} = \exp\left(A - \frac{B}{T}\right)_{(kPa)^4} \quad (6)$$

	ΔH (kJ/mol H_2)	a	E/R	A	B
C_6[a]	66.50	16.87	18.86	35.73	7.99×10^3
C_7[a]	63.20	17.17	18.86	35.21	7.60×10^3
C_8[a]					
for A_n = MX	56.51	17.32	18.86	34.13	6.79×10^3
for A_n = OX	56.95	17.89	18.86	34.21	6.85×10^3
for A_n = PX	56.70	17.01	18.86	34.16	6.81×10^3
for A_n = EX	59.66	16.96	18.86	34.63	7.17×10^3
C_9^+[a]	59.29	18.90	18.86	33.56	6.36×10^3

dx.doi.org/10.1021/ef302057k | Energy Fuels 2013, 27, 4048−4070

Table 3. continued

$$IP_n \leftrightarrow A_n + 4H_2 \quad r_{7n} = k_{7n}\left(P_{IPn} - \frac{P_{An}P_{H2}{}^4}{K_{7n}}\right) \quad k_{7n} = \underset{(kmol/(kg_{cat}\ h\ kPa))}{\exp\left(a - \frac{E}{RT}\right)} \quad K_{7n} = \underset{(kPa)^4}{\exp\left(A - \frac{B}{T}\right)} \quad (7)$$

	ΔH (kJ/mol H_2)	a	E/R	A	B
C_6[a]	68.18	16.44	18.86	36.01	8.20×10^3
C_7[a]	64.83	16.90	18.86	35.47	7.79×10^3
C_8[a]					
for A_n = MX	60.73	16.27	18.86	34.81	7.30×10^3
for A_n = OX	61.17	16.78	18.86	34.87	7.35×10^3
for A_n = PX	60.90	16.04	18.86	34.83	7.32×10^3
for A_n = EX	63.88	15.93	18.86	35.23	7.68×10^3
C_9^+[a]	60.77	17.66	18.86	34.81	7.3×10^3

[a]Reactions added into the Padmavathi et al.[42] model.

Table 4. Rate Constants and the Heat of (A) Isomerization of Naphthene and Paraffin Reactions and (B) Isomerization of Aromatic Reactions

A

$$ACP_n \leftrightarrow ACH_n \quad r_{8n} = k_{8n}\left(P_{ACPn} - \frac{P_{ACHn}}{K_{8n}}\right) \quad k_{8n} = \underset{(kmol/(kg_{cat}\ h\ kPa))}{\exp\left(a - \frac{E}{RT}\right)} \quad K_{8n} = \underset{(-)}{\exp\left(A - \frac{B}{T}\right)} \quad (8)$$

	ΔH (kJ/mol)	a	E/R	A	B
C_6	−17.10	15.11	23.81	−5.20	-2.06×10^3
C_7	−27.90	24.73	23.81	−6.63	-3.36×10^3
C_8	−29.20	25.78	23.81	−6.83	-3.51×10^3
C_9^+	−31.00	26.13	23.81	−7.16	-3.73×10^3

$$NP_n \leftrightarrow IP_n \quad r_{9n} = k_{9n}\left(P_{NPn} - \frac{P_{IPn}}{K_{9n}}\right) \quad k_{9n} = \underset{(kmol/(kg_{cat}\ h\ kPa))}{\exp\left(a - \frac{E}{RT}\right)} \quad K_{9n} = \underset{(-)}{\exp\left(A - \frac{B}{T}\right)} \quad (9)$$

	ΔH (kJ/mol)	a	E/R	A	B
C_4[a]	−9.23	25.08	26	0.80	-1.11×10^3
C_5[a]	−6.94	24.89	26	1.17	-0.83×10^3
C_6	−9.86	24.70	26	0.69	-1.19×10^3
C_7	−6.45	24.15	26	1.27	-0.76×10^3
C_8	−13.95	25.54	26	0.04	-1.68×10^3
C_9^+	−21.00	24.48	26	−1.09	-2.53×10^3

B

$$R \leftrightarrow P \quad \text{for } n = 1, \ldots, 6 \quad r_{10n} = k_{10n}\left(P_R - \frac{P_P}{K_{10n}}\right) \quad k_{10n} = \underset{(kmol/(kg_{cat}\ h\ kPa))}{\exp\left(a - \frac{E}{RT}\right)} \quad K_{10n} = \underset{(-)}{\exp\left(A - \frac{B}{T}\right)} \quad (10)$$

	R	P	ΔH (kJ/mol)	a	E/R	A	B
$n = 1$[a]	OX	PX	−10.50	25.21	21.24	12.13	-1.26×10^3
$n = 2$[a]	OX	MX	−17.60	24.50	21.24	11.00	-2.11×10^3
$n = 3$[a]	MX	EB	12.60	24.53	21.24	15.81	1.50×10^3
$n = 4$[a]	OX	EB	10.84	25.17	21.24	15.54	1.30×10^3
$n = 5$[a]	EB	PX	−11.89	25.84	21.24	11.91	-1.43×10^3
$n = 6$[a]	MX	PX	0.71	24.47	21.24	13.7	-0.085×10^3

[a]Reactions added into the Padmavathi et al.[42] model.

isomerization reactions between PX, MX, and OX occur rapidly, while isomerization between EB and xylene isomers occurs slowly. The other reaction between aromatics (transalkylation) is a reaction in which one of the alkyl groups is transferred from one alkyl aromatic molecule to another aromatic. The last two types of naphtha reactions (hydrocracking and hydrodealkylation reactions) are much slower reactions producing less valuable products than the other reactions. These reactions are exothermic, and their rates increase with increasing carbon number. The cracking of both naphthene and paraffin, as well as hydrodealkylation reactions, are irreversible.

It should be mentioned that an optimization procedure is utilized to find the unknown constants of reaction rates. These constants are determined via simultaneous minimization of the outlet temperature, molar flow rate, and coke concentration differences between the modeling results and plant data.

dx.doi.org/10.1021/ef302057k | Energy Fuels 2013, 27, 4048−4070

Table 5. Rate Constants and the Heat of Transalkylation Reactions

$$2R \leftrightarrow P + C \quad \text{for } n = 7, 8 \quad r_{11n} = k_{11n}\left(P_R^{\,2} - \frac{P_P P_C}{K_{11n}}\right) \quad \underset{(\mathrm{kmol}/(\mathrm{kg_{cat}\ h\ kPa^2}))}{k_{11n} = \exp\left(a - \frac{E}{RT}\right)} \quad \underset{(-)}{K_{11n} = \exp\left(A - \frac{B}{T}\right)} \tag{11}$$

	R	P	C	ΔH(kJ/mol)	a	E/R	A	B
$n = 7$[a]	T	B	PX	16.20	16.68	21.24	16.41	1.95×10^3
$n = 8$[a]	OX	T	A_{9+}	09.16	15.48	21.24	15.28	1.10×10^3

[a]Reactions added into the Padmavathi et al.[42] model.

Table 6. Rate Constants and the Heat of Cracking of (A) Paraffin Reactions and (B) Naphthene Reactions

A

$$\text{for } n = 2 \quad P_2 + H_2 \rightarrow 2P_1$$
$$\text{for } n = 3 \quad P_3 + H_2 \rightarrow P_1 + P_2$$
$$\text{for } n = 4 \quad NP_4 + H_2 \rightarrow \frac{2}{3}(P_3 + P_2 + P_1)$$
$$\text{for } n = 5 \quad NP_5 + H_2 \rightarrow \frac{1}{2}(NP_4 + P_3 + P_2 + P_1) \tag{12}$$

$$\text{for } n = 6\text{–}9 \quad NP_n + \frac{n-3}{3}H_2 \rightarrow \frac{n}{15}\sum_{i=1}^{5} P_i \quad r_{12n} = k_{12n}\left(\frac{P_{NPn}}{P_t}\right) \quad \underset{(\mathrm{kmol}/(\mathrm{kg_{cat}\ h}))}{k_{12n} = \exp\left(a - \frac{E}{RT}\right)}$$

	ΔH (kJ/mol)	a	E/R
C_2[a]	−65.20	37.85	34.61
C_3[a]	−53.60	39.95	34.61
C_4[a]	−49.50	40.15	34.61
C_5[a]	−47.80	41.60	34.61
C_6	−47.26	42.08	34.61
C_7	−46.69	42.48	34.61
C_8	−46.61	40.53	34.61
C_{9+}	−46.15	43.85	34.61

$$\text{for } n = 4 \quad IP_4 + \frac{3}{2}H_2 \rightarrow \frac{1}{2}(3P_1 + P_2 + P_3)$$
$$\text{for } n = 5 \quad IP_5 + H_2 \rightarrow \frac{1}{2}(IP_4 + P_3 + P_2 + P_1) \tag{13}$$

$$\text{for } n = 6\text{–}9 \quad IP_n + \frac{n-3}{3}H_2 \rightarrow \frac{n}{15}\sum_{i=1}^{5} P_i \quad r_{13n} = k_{13n}\left(\frac{P_{IPn}}{P_t}\right) \quad \underset{(\mathrm{kmol}/(\mathrm{kg_{cat}\ h}))}{k_{13n} = \exp\left(a - \frac{E}{RT}\right)}$$

	ΔH (kJ/mol)	a	E/R
C_4[a]	−40.30	36.15	34.61
C_5[a]	−45.30	41.57	34.61
C_6	−37.40	40.53	34.61
C_7	−41.85	41.57	34.61
C_8	−36.00	41.51	34.61
C_{9+}	−35.65	42.93	34.61

Table 6. continued

B

$$ACH_n + \frac{n}{3}H_2 \rightarrow \frac{n}{15}\sum_{i=1}^{5} P_i \quad r_{14n} = k_{14n}\left(\frac{P_{ACHn}}{P_t}\right) \quad \underset{(\mathrm{kmol}/(\mathrm{kg_{cat}\ h}))}{k_{14n} = \exp\left(a - \frac{E}{RT}\right)} \tag{14}$$

	ΔH (kJ/mol)	a	E/R
C_6	−45.45	42.15	34.61
C_7	−40.76	44.70	34.61
C_8	−41.00	43.90	34.61
C_{9+}	−40.10	44.15	34.61

$$\text{for } n = 5 \quad ACP_5 + 2H_2 \rightarrow \frac{1}{2}(NP_4 + P_3 + P_2 + P_1)$$
$$\text{for } n = 6\text{–}9 \quad ACP_n + \frac{n}{3}H_2 \rightarrow \frac{n}{15}\sum_{i=1}^{5} P_i \quad r_{15n} = k_{15n}\left(\frac{P_{ACPn}}{P_t}\right) \quad \underset{(\mathrm{kmol}/(\mathrm{kg_{cat}\ h}))}{k_{15n} = \exp\left(a - \frac{E}{RT}\right)} \tag{15}$$

	ΔH (kJ/mol)	a	E/R
C_5[a]	−68.74	40.23	34.61
C_6	−54.00	41.55	34.61
C_7	−52.71	43.75	34.61
C_8	−51.95	43.65	34.61
C_{9+}	−50.40	44.15	34.61

[a]Reactions added into the Padmavathi et al.[42] model.

4. CATALYST DEACTIVATION MODEL

In the reforming process, carbonaceous material or coke is deposited on the catalyst and blocks the active sites. It reduces the yield and selectivity of catalyst as the reaction proceeds. Since the coke amount is closely related to the deactivation rate, controlling coke deposition is equal to controlling catalyst deactivation.[1] The coke formation rate should be considered into the mathematical model to predict the behavior of the reactions subject to catalyst deactivation.[42] Since the catalyst of naphtha reforming process is a bifunctional catalyst containing metallic and acidic functions, in the present model, the deactivation of both metallic and acidic functions are considered. Commonly, the acidic and metallic functions are provided in the industry by chloride alumina and platinum, respectively.

dx.doi.org/10.1021/ef302057k | Energy Fuels 2013, 27, 4048−4070

Table 7. Rate Constants and the Heat of Hydrodealkylation Reactions

$$A_{n+1} + H_2 \rightarrow A_k + C_mH_{2m+2}$$

$$r_{16n} = k_{16n}P_{An+1}P_{H2}^{0.5} \quad k_{16n} = \exp\left(a - \frac{E}{RT}\right) \quad \text{(kmol/(kg}_{cat}\text{ h kPa}^{1.5}\text{))} \qquad (16)$$

	m	k	ΔH (kJ/mol)	a	E/R
C_7	1	n	−41.81	7.64	17.92
C_8					
for A_{n+1} = PX	1	n	−42.32	5.57	17.92
for A_{n+1} = EB[a]	2	$n-1$	−20.02	5.55	17.92
C_9^+					
for A_{n+1} = OX	1	n	−52.57	8.91	17.92
for A_k = T[a]	2	$n-1$	−30.80	5.57	17.92

[a]Reactions added into the Padmavathi et al.[42] model.

In order to improve the catalyst activity, stability, and selectivity, various metals such as Re, Ir, Rh, Ge, In, and Sn have been added to the metallic function. Table 8 shows the catalyst functions on the main reactions in the proposed kinetic model. The rate of coke formation generally depends on operating conditions such as pressure, temperature, and hydrogen over hydrocarbon molar ratio. In addition, alkylcyclopentane concentration is considered in some works as a factor affecting coke formation rate.[43−45] The order of concentration of alkylcyclopentane in the coke formation rate when the catalysts are fresh is considered to be 0.5.[45]

In this study, a new deactivation model is developed in which the aforementioned affecting parameters are taken into account as follows:

$$r_C^0 \propto \frac{\exp\left(-\frac{E_c}{RT}\right)}{P^{n_1}\left(\frac{H_2}{HC}\right)^{n_2}} C_{ACP}^{0.5} \qquad (17)$$

where r_C^0 is the rate of coke formation when the catalysts are fresh, E_c is coke formation activation energy, C_{ACP} is alkyl-cyclopentane concentration, and P is the pressure of reaction side. The proposed model for catalyst deactivation rate calculation based on catalyst function can be observed in Table 9. More explanations regarding the derivation of the deactivation model are provided in Appendix A.

It should be mentioned that by considering the commercial data from conventional configuration, the coke weight fraction in the output of the fourth reactor approaches 0.05. In the membrane reactors, by hydrogen extraction, the coke weight fraction becomes higher than the conventional value. Since by increasing the circulation rate the percent of coke on the catalyst can be decreased, the output coke weight fraction of the fourth membrane reactor is adjusted at 0.05 by the help of the catalyst axial velocity (the axial velocity of catalysts is increased to 0.1367 mm/s).

5. MATHEMATICAL MODELING

In this study, attempts have been made to develop an accurate mathematical model for radial-flow moving bed membrane reactor. A two-dimensional model has been taken into consideration in order to determine the concentration and temperature distributions inside the reactors. The assumptions made during the modeling of catalytic reactors are as follows:

1. The reactors operate in steady-state conditions.
2. A cross flow pattern (catalyst moves axially downward and the gas stream moves radially) is considered in the reactors.
3. Diffusion of mass and heat in both the radial and axial directions of the reactor are neglected.
4. A homogeneous catalyst moving bed is considered.
5. The gas mixtures are assumed to be ideal.
6. Heat loss is negligible.
7. The peripheral gradient (gradient along the perimeter) is neglected.
8. Intrapellet heat and mass diffusion in the catalyst pellet are ignored.
9. The effect of membrane support is neglected.
10. The membrane is just permeable for hydrogen.
11. Sievert's law is applicable.

To obtain the energy and mole balance equations, a differential element as shown in Figure 5 has been considered.

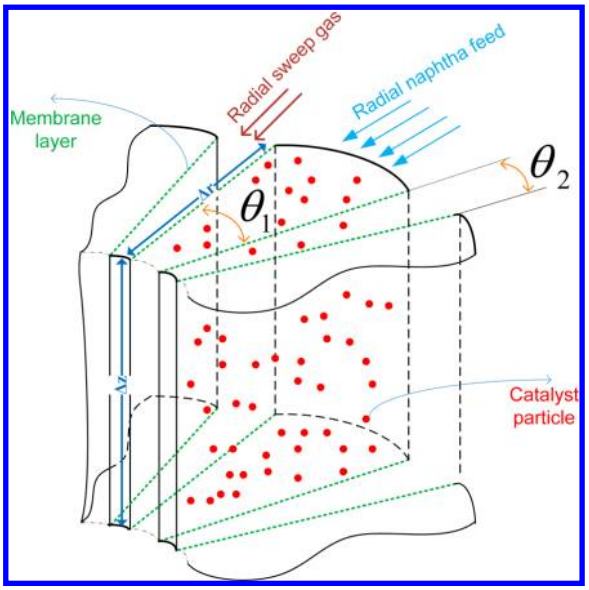

Figure 5. Differential element for mass and energy balances.

The corresponding mass and energy balance equations, pressure drop, hydrogen permeation rate, and the velocity distribution are listed in Table 10. The derivations of mass and energy balance equations and velocity distribution are provided in Appendix B.

6. NUMERICAL SOLUTION

The proposed model leads to a partial differential equations system. To solve this system, the mass and energy balance for both sweep gas and reaction sides should be coupled with the auxiliary relations. As the finite difference is one of the most commonly used methods in the simulation of membrane reactors due to its accuracy and easiness of implementation,[46,47] in the present work, the forward finite difference is employed with explicit formula to solve the set of coupled equations. In order to solve the obtained equations by this method, at first a grid of nodes should be introduced in each reactor, then the derivatives in the equations are replaced by numerical differentiation formula. The obtained algebraic equations are solved, and finally, the computer code is applied. It should be mentioned that in the explicit method, solution

dx.doi.org/10.1021/ef302057k | Energy Fuels 2013, 27, 4048−4070

Table 8. Catalyst Functions on the Main Reactions in the Proposed Kinetic Model (Metallic (M) and Acidic (A) Functions)

	reactions	agent		reactions	agent
r_{1n}	$ACH_n \leftrightarrow A_n + 3H_2$	M	r_{9n}	$NP_n \leftrightarrow IP_n$	A
r_{2n}	$ACH_n + H_2 \leftrightarrow NP_n$	M + A	r_{10n}	$R \leftrightarrow P$	A
r_{3n}	$ACH_n + H_2 \leftrightarrow IP_n$	M + A	r_{11n}	$2R \leftrightarrow P + C$	M
r_{4n}	$NP_n \leftrightarrow ACP_n + H_2$	M + A	r_{12n}	$NP_n + \frac{(n-3)}{3}H_2 \rightarrow \frac{n}{15}\sum_{i=1}^{5} P_i$	M or A
r_{5n}	$IP_n \leftrightarrow ACP_n + H_2$	M + A	r_{13n}	$IP_n + \frac{(n-3)}{3}H_2 \rightarrow \frac{n}{15}\sum_{i=1}^{5} P_i$	M or A
r_{6n}	$NP_n \leftrightarrow A_n + 4H_2$	M + A	r_{14n}	$ACH_n + \frac{n}{3}H_2 \rightarrow \frac{n}{15}\sum_{i=1}^{5} P_i$	M or A
r_{7n}	$IP_n \leftrightarrow A_n + 4H_2$	M + A	r_{15n}	$ACP_n + \frac{n}{3}H_2 \rightarrow \frac{n}{15}\sum_{i=1}^{5} P_i$	M or A
r_{8n}	$ACP_n \leftrightarrow ACH_n$	A	r_{16n}	$A_{n+1} + H_2 \rightarrow A_k + C_mH_{2m+2}$	M

Table 9. Catalyst Deactivations Model

$$r_i = a_i r_i^0 \begin{cases} \text{reaction occurs on acid function} & a_i = a_A \\ \text{reaction occurs on metal function} & a_i = a_M \\ \text{reaction occurs on acid or metal function} & a_i = \text{mean}(a_A, a_M) \\ \text{reaction occurs on acid as well as metal functions} & a_i = \text{mean}(a_A, a_M) \end{cases} \quad (18)$$

reaction occurs on metal function

$$r_i = a_M r_i^0 \quad (19)$$

$$-\frac{da_M}{dC_{C_M}} = \alpha_M a_M^{n_M} \quad (21)$$

$$\begin{cases} n_M = 1 & a_M = \exp(-\alpha_M C_{C_M}) \\ n_M \neq 1 & a_M = \dfrac{1}{(1 + (n_M - 1)\alpha_M C_{C_M})^{(1/n_M - 1)}} \end{cases} \quad (23)$$

$$r_{C_M} = a_{C_M} r_{C_M}^0 \quad (25)$$

$$-\frac{da_{C_M}}{dC_{C_M}} = \alpha_{C_M} a_{C_M}^{n_{C_M}} \quad (27)$$

$$\begin{cases} n_{C_M} = 1 & a_{C_M} = \exp(-\alpha_{C_M} C_{C_M}) \\ n_{C_M} \neq 1 & a_{C_M} = \dfrac{1}{(1 + (n_{C_M} - 1)\alpha_{C_M} C_{C_M})^{(1/n_{C_M} - 1)}} \end{cases} \quad (29)$$

$$r_{C_M}^0 = \frac{k_{C_M} \exp\left(-\frac{E_c}{RT}\right)}{P^{n_1}\left(\frac{H_2}{HC}\right)^{n_2}} C_{ACP}^{0.5} \quad (31)$$

reaction occurs on acid function

$$r_i = a_A r_i^0 \quad (20)$$

$$-\frac{da_A}{dC_{C_A}} = \alpha_A a_A^{n_A} \quad (22)$$

$$\begin{cases} n_A = 1 & a_A = \exp(-\alpha_A C_{C_A}) \\ n_A \neq 1 & a_A = \dfrac{1}{(1 + (n_A - 1)\alpha_A C_{C_A})^{(1/n_A - 1)}} \end{cases} \quad (24)$$

$$r_{C_A} = a_{C_A} r_{C_A}^0 \quad (26)$$

$$-\frac{da_{C_A}}{dC_{C_A}} = \alpha_{C_A} a_{C_A}^{n_{C_A}} \quad (28)$$

$$\begin{cases} n_{C_A} = 1 & a_{C_A} = \exp(-\alpha_{C_A} C_{C_A}) \\ n_{C_A} \neq 1 & a_{C_A} = \dfrac{1}{(1 + (n_{C_A} - 1)\alpha_{C_A} C_{C_A})^{(1/n_{C_A} - 1)}} \end{cases} \quad (30)$$

$$r_{C_A}^0 = \frac{k_{C_A} \exp\left(-\frac{E_c}{RT}\right)}{P^{n_1}\left(\frac{H_2}{HC}\right)^{n_2}} C_{ACP}^{0.5} \quad (32)$$

of each node becomes the boundary condition for the following one.

7. MODEL VALIDATION

In order to verify the efficiency of model, the predicted model results for the conventional reactors are compared with the commercial data from Nouri Petrochemical Company. Table 11 shows a comparison between the plant data and the predicted molar flow rate of components in the system output. Model results show a good agreement with the plant data. Choosing the kinetics and models for the system that underestimate true reaction rate and application of some simplifying assumptions in the mathematical modeling of process are the reasons of this minor deviation.

8. RESULTS AND DISCUSSIONS

In this section, the variation of component molar flow rates, operating conditions, and physical properties along the radial and axial directions of moving bed reactors are investigated. In the 2D plots, the variation of parameters along one of the radial or axial directions is shown by considering an average value of the parameters along the other direction. For some parameters, their variations along the axial and radial directions are shown simultaneously by the help of 3D plot. At first, the temperature profile is investigated. Figure 6 shows the temperature profiles of the conventional and membrane reactors, simultaneously. In the first reactor of both configurations, temperature decreases sharply owing to the presence of a fast endothermic reaction (dehydrogenation of naphthenes to aromatics). In the

dx.doi.org/10.1021/ef302057k | Energy Fuels 2013, 27, 4048−4070

Table 10. Mass and Energy Balances and Auxiliary Relations for the Membrane Configuration

mass balance (reaction side)

$$\frac{\partial C_j}{\partial r} = -\frac{C_j}{r} - \frac{C_j}{u_r}\frac{\partial u_r}{\partial r} + \frac{\rho_b}{u_r}\sum_{i=1}^{m} a_i \nu_{ij} r_i - \frac{\mathrm{NOS}}{\pi r R_\theta u_r}\begin{cases} 0 & j \neq \mathrm{H_2} \\ J_{\mathrm{H_2}} & j = \mathrm{H_2},\ P_{\mathrm{H_2}} \geq P^s_{\mathrm{H_2}} \\ -J_{\mathrm{H_2}} & j = \mathrm{H_2},\ P^s_{\mathrm{H_2}} > P_{\mathrm{H_2}} \end{cases} \quad \begin{matrix} j = 1, 2, \ldots, n \\ i = 1, 2, \ldots, m \end{matrix} \tag{33}$$

mass balance (sweep gas side)

$$\frac{\partial C^s_j}{\partial r} = -\frac{C^s_j}{r} - \frac{C^s_j}{u^s_r}\frac{\partial u^s_r}{\partial r} + \frac{\mathrm{NOS}}{\pi r(1-R_\theta)u^s_r}\begin{cases} 0 & j \neq \mathrm{H_2} \\ J_{\mathrm{H_2}} & j = \mathrm{H_2},\ P_{\mathrm{H_2}} \geq P^s_{\mathrm{H_2}} \\ -J_{\mathrm{H_2}} & j = \mathrm{H_2},\ P^s_{\mathrm{H_2}} > P_{\mathrm{H_2}} \end{cases} \quad j = 1, 2, \ldots, n' \tag{34}$$

energy balance (reaction side)

$$\frac{\partial T}{\partial r} = -\frac{\rho_b}{u_r C_T C_P}\sum_{i=1}^{m}(\Delta H_i a_i r_i) + \frac{\mathrm{NOS}}{\pi r R_\theta u_r C_T C_P}U(T^s - T) + \frac{\mathrm{NOS}}{\pi r R_\theta u_r C_T C_P}\begin{cases} J_{\mathrm{H_2}}(H_{\mathrm{H_2}} - H_{\mathrm{H_2}}) & P_{\mathrm{H_2}} \geq P^s_{\mathrm{H_2}} \\ J_{\mathrm{H_2}}(-H_{\mathrm{H_2}} + H^s_{\mathrm{H_2}}) & P^s_{\mathrm{H_2}} > P_{\mathrm{H_2}} \end{cases} \tag{35}$$

energy balance (sweep gas side)

$$\frac{\partial T^s}{\partial r} = \frac{\mathrm{NOS}}{\pi r(1-R_\theta)u^s_r C^s_T C_P}U(T - T^s) - \frac{\mathrm{NOS}}{\pi r(1-R_\theta)u^s_r C^s_T C_P}\begin{cases} J_{\mathrm{H_2}}(H_{\mathrm{H_2}} - H_{\mathrm{H_2}}) & P_{\mathrm{H_2}} \geq P^s_{\mathrm{H_2}} \\ J_{\mathrm{H_2}}(-H_{\mathrm{H_2}} + H^s_{\mathrm{H_2}}) & P^s_{\mathrm{H_2}} > P_{\mathrm{H_2}} \end{cases} \tag{36}$$

hydrogen permeation rate

$$J_{\mathrm{H_2}} = \frac{Q_0 \exp\left(-\frac{E_{\mathrm{H_2}}}{RT}\right)}{\delta_{\mathrm{H_2}}}(|\sqrt{P_{\mathrm{H_2}}} - \sqrt{P^{\mathrm{sweep}}_{\mathrm{H_2}}}|) \tag{37}$$

$Q_0 = 1.65 \times 10^{-5}$ mol/(m s kPa$^{1/2}$)

$E_{\mathrm{H_2}} = 15.7$ kJ/mol

velocity distribution (reaction side)

$$\frac{\partial u_r}{\partial r} = -\frac{u_r}{r} - \frac{u_r}{C_T}\frac{\partial C_T}{\partial r} + \frac{\rho_b}{C_T}\sum_{j=1}^{n}\sum_{i=1}^{m} a_i \nu_{ij} r_i - \frac{\mathrm{NOS}}{\pi r R_\theta C_T}\begin{cases} J_{\mathrm{H_2}} & P_{\mathrm{H_2}} \geq P^s_{\mathrm{H_2}} \\ -J_{\mathrm{H_2}} & P^s_{\mathrm{H_2}} > P_{\mathrm{H_2}} \end{cases} \tag{38}$$

velocity distribution (sweep gas side)

$$\frac{\partial u^s_r}{\partial r} = -\frac{u^s_r}{r} - \frac{u^s_r}{C^s_T}\frac{\partial C^s_T}{\partial r} + \frac{\mathrm{NOS}}{\pi r(1-R_\theta)C^s_T}\begin{cases} J_{\mathrm{H_2}} & P_{\mathrm{H_2}} \geq P^s_{\mathrm{H_2}} \\ -J_{\mathrm{H_2}} & P^s_{\mathrm{H_2}} > P_{\mathrm{H_2}} \end{cases} \tag{39}$$

collector (reaction side)

$$\frac{\partial F_j}{\partial z} = \frac{2\pi R_i}{\mathrm{NOS}}u_{re}C_{je}R_\theta \quad j = 1, 2, \ldots, n$$

$$\frac{\partial T}{\partial z} = \frac{1}{F_T C_P}\frac{2\pi R_i}{\mathrm{NOS}}C_{Te}u_{re}R_\theta C_{P_e}(T_e - T) - \frac{T}{F_T}\left(\frac{2\pi R_i}{\mathrm{NOS}}u_{re}R_\theta C_{Te}\right) - \frac{T}{C_P}\frac{\partial C_P}{\partial z} \tag{40}$$

collector (sweep gas side)

$$\frac{\partial F^s_j}{\partial z} = \frac{2\pi R_i}{\mathrm{NOS}}u^s_{re}C^s_{je}(1-R_\theta) \quad j = 1, 2, \ldots, n'$$

$$\frac{\partial T^s}{\partial z} = \frac{C^s_{Te}u^s_{re}}{F^s_T C_P}\frac{2\pi R_i}{\mathrm{NOS}}(1-R_\theta)C_{P_e}(T^s_e - T^s) - \frac{T^s}{F^s_T}\left(\frac{2\pi R_i}{\mathrm{NOS}}u^s_{re}(1-R_\theta)C^s_{Te}\right) - \frac{T^s}{C_P}\frac{\partial C_P}{\partial z} \tag{41}$$

ergun equation (pressure drop)

$$\frac{\mathrm{d}P}{\mathrm{d}r} = \frac{150\mu}{\phi_s^2 d_p^2}\frac{(1-\varepsilon)^2}{\varepsilon^3}u_r + \frac{1.75\rho}{\phi_s d_p}\frac{(1-\varepsilon)}{\varepsilon^3}u_r^2 \tag{42}$$

additional relations

$$R_\theta = \frac{\theta_1}{\theta_1 + \theta_2} \tag{43}$$

membrane reactor, a higher temperature drop is seen because hydrogen extraction shifts the dehydrogenation reaction toward the product side. Therefore, more heat is consumed and higher temperature drop appears. The outlet stream of the reactor is heated by the furnace; thus, a sudden jump in the plot is observed. Compared with the first reactors of CR and MR configurations, a lower temperature reduction is seen in the second reactors where the remaining naphthenes are converted

dx.doi.org/10.1021/ef302057k | Energy Fuels 2013, 27, 4048−4070

Table 11. Comparison between Predicted Production Rate and Plant Data

pseudocomponents	molecular weight	input plant (mole fraction)	output plant (kmol/h)	output model (kmol/h)	deviation (kmol/h)
n-P_6 (C_6H_{14})	86.178	0.0229	71.84	70.98	0.86
n-P_7 (C_7H_{16})	100.205	0.0292	46.65	46	0.65
n-P_8 (C_8H_{18})	114.232	0.0239	8.1	7.63	0.47
n-P_9 (C_9H_{20})	128.259	0.0156	1.15	1.25	−0.1
i-P_6 (C_6H_{14})	86.178	0.0232	216.06	216.06	0
i-P_7 (C_7H_{16})	100.25	0.0314	110.18	109.69	0.49
i-P_8 (C_8H_{18})	114.232	0.0338	22.75	22.67	0.08
i-P_9 (C_9H_{20})	128.259	0.0244	1.79	1.95	−0.16
ACH_6 (C_6H_{12})	84.162	0.0077	0.51	0.92	−0.41
ACH_7 (C_7H_{14})	98.189	0.0084	0.92	1.43	−0.51
ACH_8 (C_8H_{16})	112.216	0.0115	2.33	2.34	−0.01
ACH_9 (C_9H_{18})	126.243	0.0018	0.04	0.05	−0.01
ACP_5 (C_5H_{10})	70.135	0.0001	2.14	2.11	0.03
ACP_6 (C_6H_{12})	84.162	0.003	26	26.02	−0.02
ACP_7 (C_7H_{14})	98.189	0.0065	2.33	3.12	−0.79
ACP_8 (C_8H_{16})	112.216	0.0084	0.6	0.6	0
ACP_9 (C_9H_{18})	126.243	0.0012	0.01	0.02	−0.01
A_6 (C_6H_6)	78.114	0.0086	205.84	206.39	−0.55
A_7 (C_7H_8)	92.141	0.0109	453.93	454.33	−0.4
A_8 (C_8H_{10})	106.168	0.0021	163.02	163.47	−0.45
A_9 (C_9H_{12})	120.195	0.0026	323.66	324.46	−0.8
A_8 (C_8H_{10})	106.168	0.0015	113.62	113.4	0.22
A_8 (C_8H_{10})	106.168	0.0016	120.84	121.55	−0.71
A_8 (C_8H_{10})	106.168	0.0036	276.56	276.8	−0.24
H_2	2.016	0.6226	10071.31	10090.82	−19.51
P_1 (CH_4)	16.043	0.0211	398.53	396.64	1.89
P_2 (C_2H_6)	30.07	0.0231	399.16	397.72	1.44
P_3 (C_3H_8)	44.097	0.0202	352.36	351.69	0.67
P_4 (C_4H_{10})	58.124	0.0106	189.21	189.93	−0.72
P_5 (C_5H_{12})	72.151	0.0035	71.06	71.69	−0.63
i-P_4	58.124	0.0073	140.75	139.38	1.37
i-P_5	72.151	0.0076	149.21	149.49	−0.28

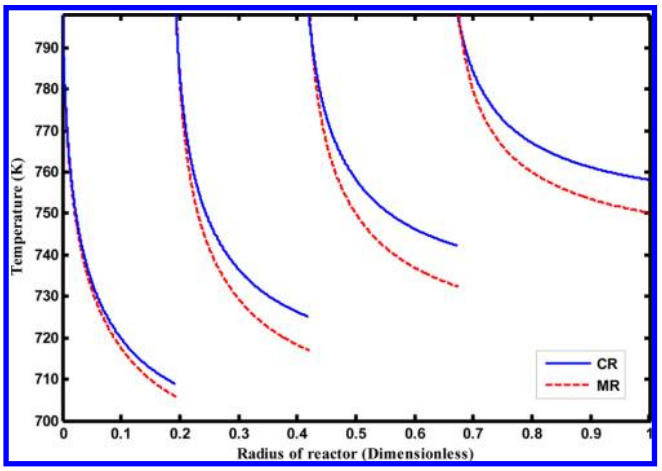

Figure 6. Temperature profile of CR and MR.

to the aromatics. Due to hydrogen extraction, the higher temperature drop in the membrane reactor is logical. In the last two reactors, dehydrocyclization of paraffins to naphthenes and dehydrogenation of naphthenes to aromatics, which are endothermic, cause a temperature reduction but this temperature reduction is moderated because of increasing the degree of hydrocracking of paraffins and naphthenes, and hydrodealkylation (exothermic reactions). In the last two membrane reactors, by hydrogen removal, the dehydrogenation and dehydrocyclization are shifted toward consumption of more heat. However, by decreasing the hydrogen content, the reactant of hydrocraking and hydrodealkylation reactions decreases and less heat is generated; therefore, the temperature drop is less moderated.

One of the main goals of the newer design of reforming units is the increase of aromatics yield because the octane number (RON) of aromatic components (except for benzene) is always above 100.[1] Figure 7 shows the aromatics molar flow rate vs the

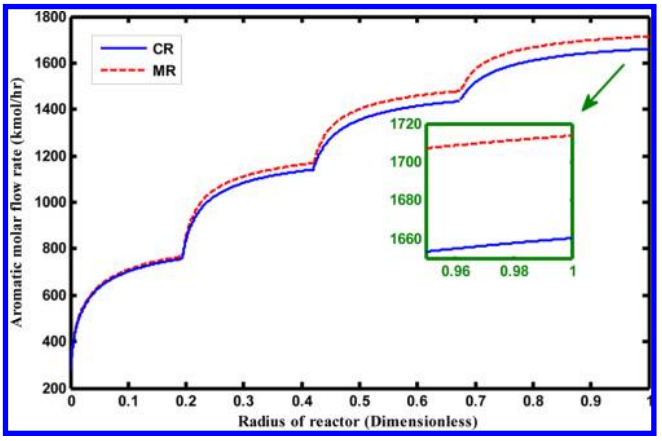

Figure 7. Aromatics molar flow rates vs the radius of conventional and membrane reactors.

radius of the reactors. As the feedstock passes through the radius of reactors, the reactions proceed and the aromatics

dx.doi.org/10.1021/ef302057k | *Energy Fuels* 2013, 27, 4048−4070

content increases. In the first two reactors, the rate of aromatics production is higher than the last two, owing to the dehydrogenation of naphthenes to aromatics reactions (the predominate reaction in the first two reactors). When the hydrogen is extracted by the membrane, the thermodynamic equilibrium shifts toward the product of naphthenes dehydrogenation reaction (aromatics); therefore, more aromatics can be obtained in comparison with the conventional system.

Another significant limitation for the newer design of reforming units is hydrogen yield improvement. Figure 8

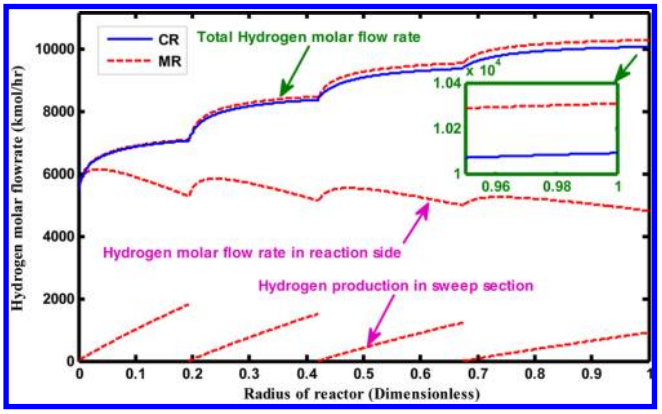

Figure 8. Hydrogen molar flow rate in both reaction and sweep gas sides for the membrane reactors.

shows the hydrogen molar flow rate in both reaction and sweep gas sides for the membrane reactors. As well, this figure shows a comparison between the total hydrogen production in MR and CR. In MR, due to hydrogen extraction, the naphthene dehydrogenation and paraffin dehydrocylization reactions shift toward the product side and consequently, more hydrogen can be achieved. Thus, as seen in the plot, the total amount of produced hydrogen (the summation of hydrogen in the sweep gas and reaction sides) in MR is about 220 kmol/h more than CR. The hydrogen permeation in the sweep section decreases from the first reactor to the fourth, owing to decreasing the partial pressure of hydrogen in the reaction side. In the initial reactors, due to high rate of hydrogen producer reactions such as dehydrogenation and dehydrocyclization, high quantity of hydrogen is produced but decreasing the rate of these reactions, as well as increasing the degree of hydrogen consumer reactions such as hydrocracking and hydrodealkylation leads to a decrease in the production of hydrogen.

The naphthenes, paraffins, and light ends molar flow rates are illustrated in Figure 9a–c. Naphthenes and paraffins constitute the major part of naphtha (typical straight-run naphtha is made up of 40–70 wt % paraffins and 20–50% naphthenes). Due to the dehydrogenation of naphthenes to aromatics and dehydrocylization of paraffins to aromatics, naphthenes and paraffins have great importance in the reforming process. A comparison between the contents of naphthenes in MR and CR is depicted in Figure 9a. Since the naphthenes are significantly consumed in the first two reactors due to dehydrogenation reaction, the plot shows a sharply decreasing trend. The result shows that consumption of naphthenes in MR is greater than CR. As previously mentioned, removing hydrogen shifts the dehydrogenation of naphthene toward the production side, for this reason more naphthene is consumed in MR. The flow rate of paraffins can be observed

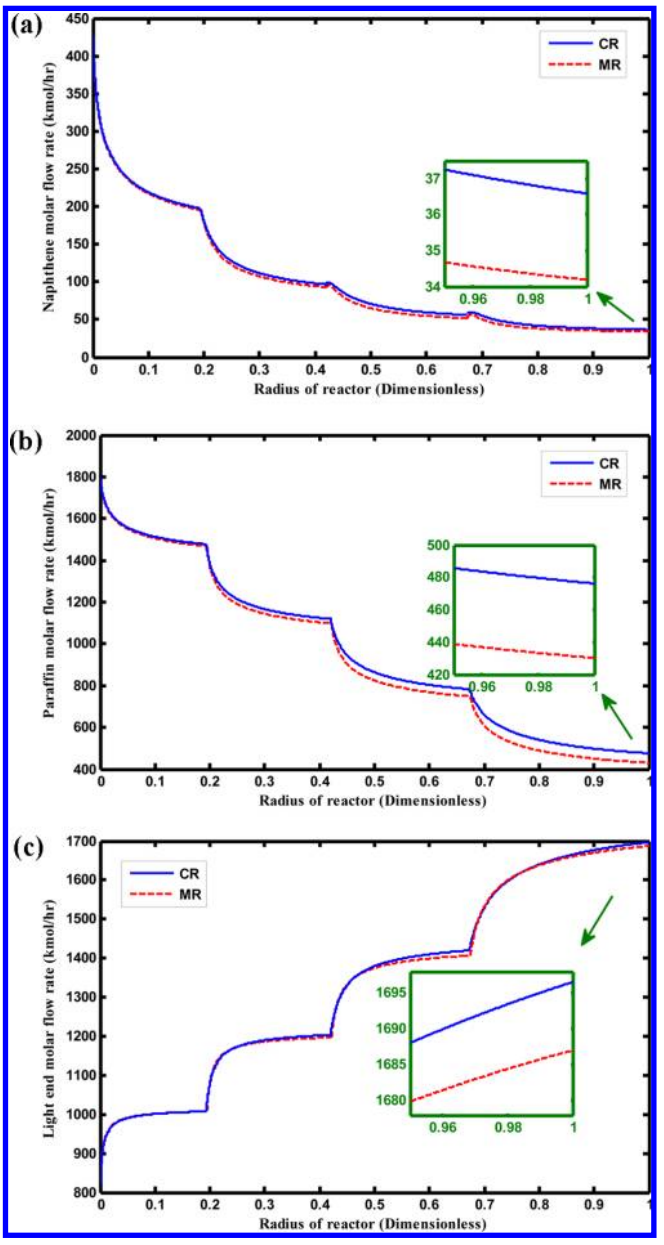

Figure 9. (a) Naphthenes, (b) paraffins, and (c) light ends molar flow rates along the radius of conventional and membrane reactors.

in the Figure 9b. As can be seen, the paraffins molar flow rate, due to dehydrocyclization and hydrocracking reactions, declines continuously along the radius of reactors. In MR, more paraffins are consumed. Because when hydrogen is extracted, dehydrocyclization of paraffins shifts toward consumption of more paraffins. The light ends molar flow rate is plotted in Figure 9c. The light end gases contain the light byproduct which is mainly produced by the hydrocracking reactions. As can be seen in the plot, the rate of light ends production in MR is lower than CR. This result is logical because hydrogen extraction leads to a decrease in hydrocracking progress and less light ends are produced.

The physical properties (molecular weight and heat capacity) along the radius of reactors are depicted in Figure 10. A comparison between the mean molecular weight of components along the radius of the membrane and conventional reactors is depicted in Figure 10a. As can be seen, the CR plot shows a decreasing trend owing to producing light

dx.doi.org/10.1021/ef302057k | Energy Fuels 2013, 27, 4048–4070

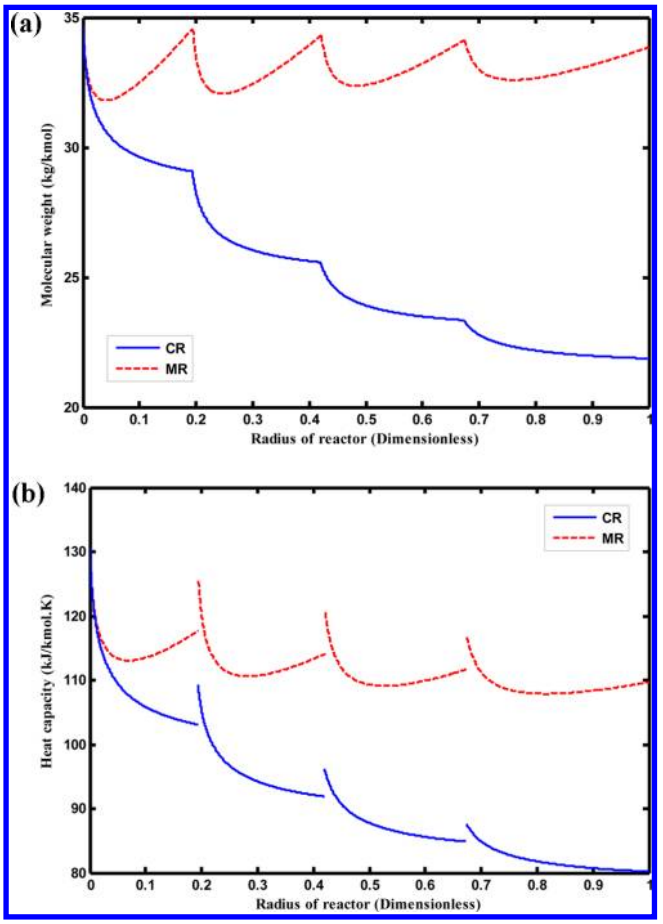

Figure 10. Comparison between (a) molecular weight and (b) heat capacity of components along the radius of the membrane and conventional reactors.

components such as hydrogen and light ends, as well as cracking of heavy components to the lighter ones. In each reactor of MR configuration, at first due to production of light components, the mean molecular weight decreases but hydrogen extraction decreases the percent of light components extremely and the mean molecular weight increases. As MR produces less light ends and removes the hydrogen from the reaction side, the components in its reaction side have a higher molecular weight. Figure 10b shows the heat capacity of the components in MR and CR. The temperature has a direct effect on heat capacity. Since the temperature decreases along the radius of each reactor of CR, a decreasing trend of heat capacity is observed. A sudden jump at the entrance of the last three reactors is due to preheating the outlet stream of the previous reactor. Unlike CR, in that its plot in each reactor only decreases, the MR plot has an increasing trend after its decrease. At first, a temperature drop leads to a decrease in the heat capacity. Then, by hydrogen (a component with a low value of heat capacity) extraction, the percentage of components with a higher value of heat capacity increases and as a consequence, the amount of the heat capacity enhances.

H_2/HC molar ratio vs the axial and radial coordinates of both CR and MR is depicted in Figure 11. H_2/HC is a controlling parameter in the naphtha reforming process. This ratio should not be lower than 2.193 (the inlet amount of the first reactor). This work has been performed by regulating the number of subsections. The low ratio of H_2/HC produces more coke

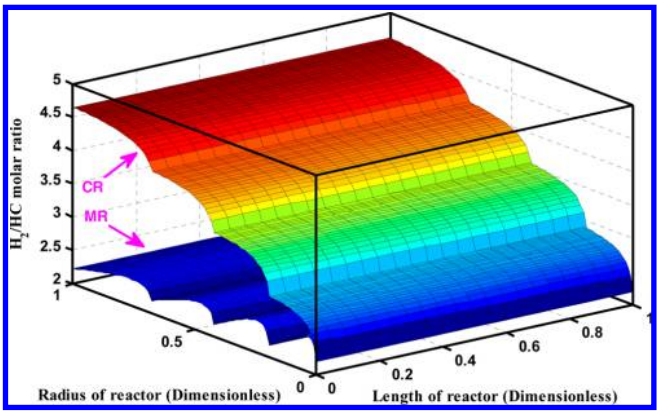

Figure 11. H_2/HC molar ratio vs the axial and radial coordinates of both CR and MR.

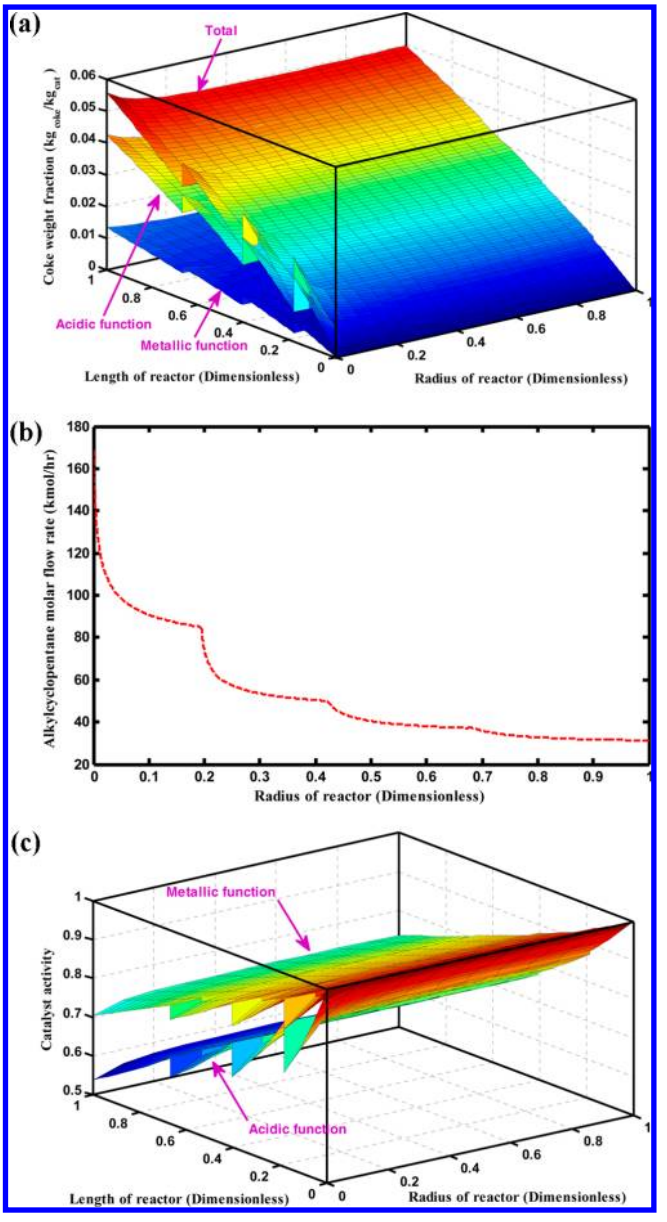

Figure 12. (a) Coke weight fractions along the length and radius of the membrane reactor for both acidic and metallic functions, (b) ACP concentration vs the radius of MR, and (c) activity of catalysts for MR.

dx.doi.org/10.1021/ef302057k | *Energy Fuels* 2013, 27, 4048−4070

deposition on the surface of the catalyst. The 3D plot shows that the H_2/HC ratio increases along the radius of the conventional reactor. Since H_2 is one of the reaction products in the reforming process that has a great production rate, its amount and H_2/HC ratio increase by reaction progression. In the membrane reactors, at first hydrogen production leads to an increase in H_2/HC molar ratio, but afterward because of hydrogen extraction, this ratio decreases.

Figure 12a shows the coke weight fraction along the length and radius of the membrane reactor for both acidic and metallic functions. Catalyst deactivation, which is generated by coke deposition, generally increases by an increase in the temperature. Along the length of the reactor, coke deposition increases because when the catalyst pellets moves axially, they are coked continuously owing to reactions progress. Unlike the axial direction, along the radius of the reactors the amount of coke on the catalysts declines. The temperature and ACP concentration are the most effective parameters that affect the rate of coke deposition. The temperature and the ACP concentration, as shown in Figures 6 and 12b, respectively, decline along the radius of reactors and cause a decrease in the rate of coke deposition. The ACP concentration decreases along the radius of reactors because ACP is consumed as the naphtha reactions progress. As previously mentioned, the outlet catalysts of one reactor are introduced to the next reactor as an inlet catalysts, but as shown in Figure 12a, the amounts of coke deposition are different in the outlet and inlet streams. This difference is due to the fact that the catalyst pellets is transported by gas lift. At the end of the reactors, the catalyst pellets have different coke content depending on their distance from the collector. When these pellets with different coke deposition are mixed together, the use of an average amount of coke weight fraction in the inlet of the next reactor is reasonable. Figure 12c shows an inverse trend for activity of the catalysts because by increasing the coke deposition a decrease in the activity of catalysts appears.

By considering the commercial data, the coke weight fraction in the output of the fourth reactor approaches 0.05. Figure 13

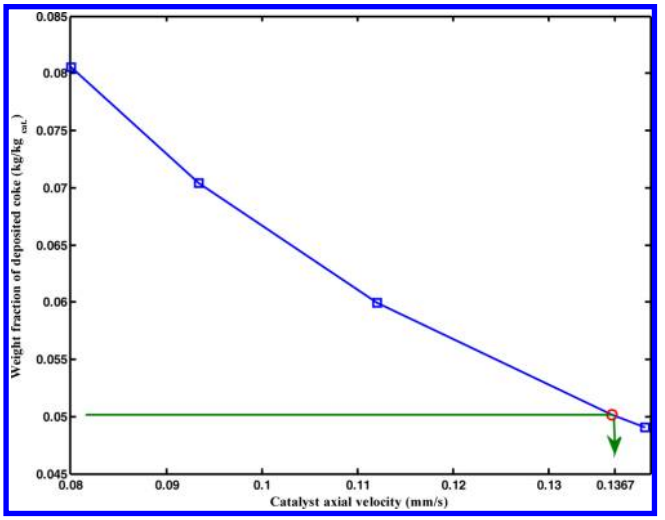

Figure 13. Weight fraction of deposited coke vs axial velocity.

shows the mean weight fraction of deposited coke along the radius of reactor vs axial velocity. As shown in the figure, the axial velocity of catalysts becomes 0.1367 (mm/s) to reduce the weight fraction of deposited coke to the conventional value (0.05) in the exit of fourth reactor.

A comparison between CR and MR coke weight fractions vs the axial direction is made in Figure 14a. The lower H_2/HC

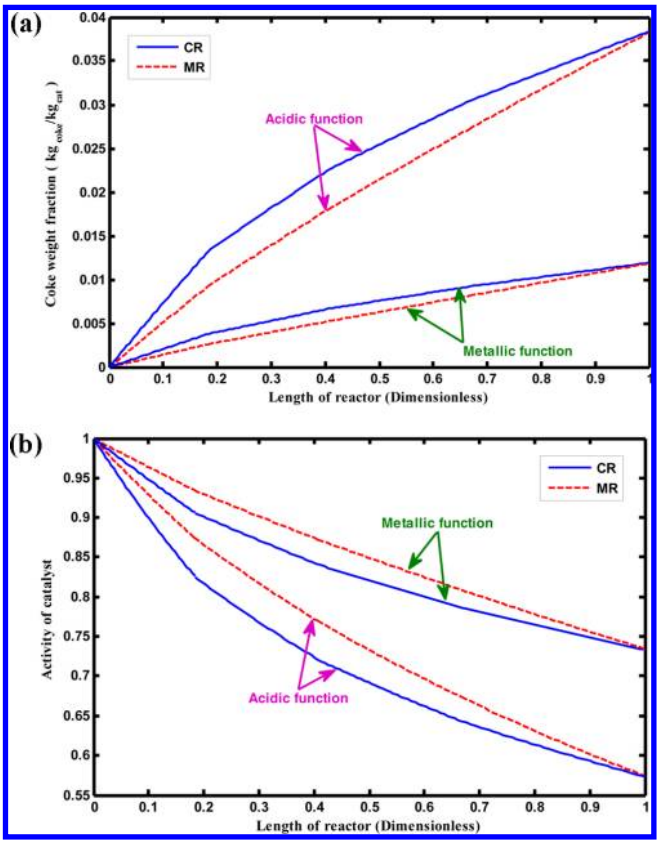

Figure 14. Comparison between CR and MR (a) coke weight fractions and (b) activity of catalysts.

ratio of MR compared with CR leads to higher coke deposition, while the lower temperature and ACP concentration, as well as the higher catalyst axial velocity, result in lower coke deposition in MR. Since the temperature, ACP concentration, and the catalyst axial velocity have a greater effect on coke weight fractions in comparison with H_2/HC ratio, less coke weight fraction can be seen in the membrane reactor compared to the conventional one. An inverse trend for the activity of catalysts is seen in Figure 14b. Since the coke content in MR is lower than conventional reactor, it has a higher catalyst activity.

9. CONCLUSIONS

In this work, a new configuration is recommended for CCR moving bed reactors. The Pd−Ag membrane layer is utilized in the moving bed reactors to boost the hydrogen and aromatics contents. The design of reactors in the membrane configuration is such that the cross-sectional area of each reactor is divided into some subsections and a radial sweep gas stream is applied to collect the hydrogen which is permeated via the membrane layers. A two-dimensional model accompanied with a new reaction network and a new deactivation model is used for simulation of the CCR moving bed reactors. In the membrane configuration the separated hydrogen can be used in the other units without requiring excess investments to separate hydrogen from other streams. The operating temperature in the

dx.doi.org/10.1021/ef302057k | Energy Fuels 2013, 27, 4048−4070

membrane reactor decreases owing to the increase in the yield of endothermic reactions. By membrane application, the coke deposition increases, but by increasing the catalyst axial velocity, the coke content in the exit of fourth reactor becomes the same as a conventional value. The results show that the membrane configuration improves the hydrogen and aromatics production noticeably. As improvments in the hydrogen and aromatics contents are both considered the limitation for newer designs of reforming units, the proposed membrane configuration could be beneficial for the CCR process.

APPENDIX A

Developing the Catalyst Deactivation Model

The reaction rate of pseudo-component i based on the activity of the catalyst and the reaction rate of the fresh catalyst can be presented as follows:

$$r_i = a_i r_i^0 \tag{A.1}$$

where (a_i) is define as

$$\begin{cases} \text{reaction occurs on acidic function} & a_i = a_A \\ \text{reaction occurs on metallic function} & a_i = a_M \\ \text{reaction occurs on acidic or metallic function} & a_i = \text{mean}(a_A, a_M) \\ \text{reaction occurs on acidic as well as metallic functions} & a_i = \text{mean}(a_A, a_M) \end{cases}$$

Thus, the reaction rate that is catalyzed by metallic function could be written as follows:

$$r_i = a_M r_i^0 \tag{A.2}$$

Metallic function activity is a function of the weight fraction of deposited coke on metallic function of the catalyst. Thus a_M is defined as follows:

$$-\frac{da_M}{dC_{C_M}} = \alpha_M a_M^{n_M} \tag{A.3}$$

where α_M is a constant and n_M is a power number of metallic function activity. α_M and n_M is determined via minimization of the difference between the plant data and modeling output. Then with integration of the recent equation, we have

$$\begin{cases} \text{if } n_M = 1 \quad a_M = \exp\left(-\alpha_M C_{C_M}\right) \\ \text{if } n_M \neq 1 \quad a_M = \dfrac{1}{\left(1 + (n_M - 1)\alpha_M C_{C_M}\right)^{(1/n_M - 1)}} \end{cases} \tag{A.4}$$

In order to calculate C_{C_M}, the mass balance for coke on metallic function should be written along the length direction. In order to achieve this end, the following trend is applied.

The coke balance on the metallic function along the z direction is considered as follows:

$$F_{C_M}|_z - F_{C_M}|_{z+dz} + r_{C_M}(\rho_b 2\pi r \Delta r\, dz) = 0 \tag{A.5}$$

By considering the Taylor's extension, the above equation becomes

$$\frac{\partial F_{C_M}}{\partial z} = r_{C_M}(\rho_b 2\pi r \Delta r) \tag{A.6}$$

where F_{C_M} and r_{C_M} are the mass flow rate of coke and the rate of coke formation on the metallic function of catalyst. In addition, F_{C_M} can be defined as follows:

$$F_{C_M} = C_{C_M} \dot{m}_{cat} \tag{A.7}$$

The mass flow rate of catalyst is defined by the following:

$$\dot{m}_{cat} = \rho_b 2\pi r \Delta r u_z \tag{A.8}$$

By substituting the above equation in eq A.7

$$F_{C_M} = C_{C_M}(\rho_b 2\pi r \Delta r u_z) \tag{A.9}$$

Then, eq A.9 is replaced in eq A.6:

$$u_z \frac{\partial C_{C_M}}{\partial z} = r_{C_M} \tag{A.10}$$

By rearranging the above equation, we have

$$\frac{\partial C_{C_M}}{\partial z} = \frac{r_{C_M}}{u_z} \tag{A.11}$$

Thus, the coke weight fraction on the metallic function (C_{C_M}) depends on the rate of coke formation on the metallic function of spent catalyst (r_{C_M}) and catalyst velocity (u_z). The term r_{C_M} is defined as follows:

$$r_{C_M} = a_{C_M} r_{C_M}^0 \tag{A.12}$$

Where $r_{C_M}^0$ is rate of coke formation on metallic function of fresh catalyst which is defined by the following:

$$r_{C_M}^0 = \frac{k_{C_M} \exp\left(-\frac{E_c}{RT}\right)}{P^{n_1}\left(\frac{H_2}{HC}\right)^{n_2}} C_{ACP}{}^{0.5} \tag{A.13}$$

In addition, a_{C_M} could be calculated by the following:

$$-\frac{da_{C_M}}{dC_{C_M}} = \alpha_{C_M} a_{C_M}^{n_{C_M}} \tag{A.14}$$

The terms n_{C_M} and α_{C_M}, like unknown constants in eq A.3, are determined via minimization of the difference between the plant data and modeling output. With integration from eq A.14, we have

$$\begin{cases} \text{if } n_{C_M} = 1 \quad a_{C_M} = \exp(-\alpha_{C_M} C_{C_M}) \\ \text{if } n_{C_M} \neq 1 \quad a_{C_M} = \dfrac{1}{(1 + (n_{C_M} - 1)\alpha_{C_M} C_{C_M})^{(1/n_{C_M} - 1)}} \end{cases} \tag{A.15}$$

By substituting eqs A.15 and A.13 in eq A.12, the rate of coke formation on the metallic function is calculated. Then by substituting the coke formation rate in eq A.11, coke weight fraction on the metallic function (C_{C_M}) could be calculated. With same procedure, reaction rates that are catalyzed by acidic site could be achieved. The results are shown in Table 10. In addition, required constants to calculate catalyst deactivation rate and activity are presented in Table A1.

dx.doi.org/10.1021/ef302057k | Energy Fuels 2013, 27, 4048−4070

Table A1. Required Constants for Calculating Catalyst Deactivation Rate and Activity

parameter	value	dimension
n_M	1	
α_M	26	kg_{cat}/kg_{coke}
n_{C_M}	1	
α_{C_M}	12.34	kg_{cat}/kg_{coke}
n_A	1	
α_A	14.5	kg_{cat}/kg_{coke}
n_{C_A}	1	
α_{C_A}	10.18	kg_{cat}/kg_{coke}
k_{C_M}	0.384	$(kg_{coke}\ kPa^{n_1}\ m^{1.5})/(kg_{cat}\ kmol^{0.5})$
k_{C_A}	1.386	$(kg_{coke}\ kPa^{n_1}\ m^{1.5})/(kg_{cat}\ kmol^{0.5})$
E_c	4055	J/mol
n_1	0.94	
n_2	1.33	

APPENDIX B: DEVELOPING THE GOVERNING EQUATIONS

Here the derivations of mass and energy balances, velocity distribution, and coke formation are presented.

Mass Balance on the Reaction Side

By considering Sivert's law, the permeated hydrogen molar flux is defined as follows:

$$J_{H_2} = \frac{Q_0 \exp\left(-\frac{E_{H_2}}{RT}\right)}{\delta_{H_2}}\left(\left|\sqrt{P_{H_2}} - \sqrt{P_{H_2}^{sweep}}\right|\right) \tag{B.1}$$

The mass balance for a control volume with length of dz and cross-sectional area defined below formula is as follows:

cross-sectional area

$$\frac{2\pi r}{NOS}\Delta r R_\theta$$

$$\begin{aligned}&\text{input} - \text{output} + \text{consumption}\\ &\quad + \text{permeation through the membrane}\\ &= \text{accumulation}\end{aligned} \tag{B.2}$$

$$(N_j A_r)|_r - (N_j A_r)|_{r+dr} + \rho_b \sum_{i=1}^{m} a_i \nu_{ij} r_i A_r\ dr - 2A_p \begin{cases} 0 & j \neq H_2 \\ J_{H_2} & j = H_2,\ P_{H_2} \geq P_{H_2}^s = \dfrac{\partial n_j}{\partial t} \\ -J_{H_2} & j = H_2,\ P_{H_2}^s > P_{H_2} \end{cases} \quad \begin{matrix} j = 1, 2, ..., n \\ i = 1, 2, ..., m \end{matrix} \tag{B.3}$$

In the above-mentioned equation, j and i refer to the number of components and reactions, respectively. Also n_j is the moles of component j in the control volume. The Pd−Ag membrane is permeable just for hydrogen and insulated for other component.

By writing the Taylor's extension of the second term on the left-hand side of the equation, the mass balance becomes

$$-\frac{\partial(N_j A_r)}{\partial r}\,dr + \rho_b \sum_{i=1}^{m} a_i \nu_{ij} r_i A_r\ dr - 2A_p \begin{cases} 0 & j \neq H_2 \\ J_{H_2} & j = H_2,\ P_{H_2} \geq P_{H_2}^s = \dfrac{\partial n_j}{\partial t} \\ -J_{H_2} & j = H_2,\ P_{H_2}^s > P_{H_2} \end{cases} \tag{B.4}$$

Now the mass balance equation is divided by the term A_r dr.

$$-\frac{1}{A_r}\frac{\partial(N_j A_r)}{\partial r} + \rho_b \sum_{i=1}^{m} a_i \nu_{ij} r_i - \frac{2A_p}{A_r\ dr} \begin{cases} 0 & j \neq H_2 \\ J_{H_2} & j = H_2,\ P_{H_2} \geq P_{H_2}^s = \dfrac{1}{A_r\ dr}\dfrac{\partial n_j}{\partial t} \\ -J_{H_2} & j = H_2,\ P_{H_2}^s > P_{H_2} \end{cases} \tag{B.5}$$

The concentration of component j in the control volume is equal to the moles of component j in the volume of the fluid. The volume of the fluid is ε times the volume of the control volume element:

$$C_j = \frac{n_j}{(A_r\ dr\varepsilon)} \tag{B.6}$$

or

$$n_j = C_j(A_r\ dr\varepsilon) \tag{B.7}$$

The cross-sectional area is obtained as follows:

$$A_r = \frac{2\pi r\ dz}{NOS}\frac{\theta_1}{\theta_1 + \theta_2} \tag{B.8}$$

and

$$R_\theta = \frac{\theta_1}{\theta_1 + \theta_2} \tag{B.9}$$

Substituting eq B.9 into B.8, the cross-sectional area is defined as follows:

$$A_r = \frac{2\pi r\ dz}{NOS}R_\theta \tag{B.10}$$

The available side area for permeation is as follows:

$$A_p = dr\ dz \tag{B.11}$$

Applying the above equations, the mass balance equation can be obtained as follows:

$$-\frac{1}{A_r}\frac{\partial(N_j A_r)}{\partial r} + \rho_b \sum_{i=1}^{m} a_i \nu_{ij} r_i - \frac{NOS}{\pi r R_\theta} \begin{cases} 0 & j \neq H_2 \\ J_{H_2} & j = H_2,\ P_{H_2} \geq P_{H_2}^s = \varepsilon\dfrac{\partial C_j}{\partial t} \\ -J_{H_2} & j = H_2,\ P_{H_2}^s > P_{H_2} \end{cases} \tag{B.12}$$

in which N_j is molar flux of component j. The molar flux comprises two terms, one due to the bulk motion and the other one for diffusion of component j which is as follows:

dx.doi.org/10.1021/ef302057k | Energy Fuels 2013, 27, 4048−4070

$$N_j = -D_{ej}\frac{\partial C_j}{\partial r} + C_j u_r \tag{B.13}$$

The above equation can be rewritten as follows:

$$N_j A_r = -A_r D_{ej}\frac{\partial C_j}{\partial r} + A_r C_j u_r \tag{B.14}$$

Substitution into the governing mass balance equation gives

$$D_{ej}\frac{1}{A_r}\frac{\partial}{\partial r}\left(A_r\frac{\partial C_j}{\partial r}\right) - \frac{1}{A_r}\frac{\partial}{\partial r}(A_r u_r C_j) + \rho_b\sum_{i=1}^{m} a_i\nu_{ij}r_i - \frac{\mathrm{NOS}}{\pi r R_\theta}\begin{cases}0 & j \neq \mathrm{H_2}\\ J_{\mathrm{H_2}} & j = \mathrm{H_2},\ P_{\mathrm{H_2}} \geq P^s_{\mathrm{H_2}} = \varepsilon\dfrac{\partial C_j}{\partial t}\\ -J_{\mathrm{H_2}} & j = \mathrm{H_2},\ P^s_{\mathrm{H_2}} > P_{\mathrm{H_2}}\end{cases}\quad \begin{matrix}j = 1, 2, ..., n\\ i = 1, 2, ..., m\end{matrix} \tag{B.15}$$

As the CCR process is steady state and diffusion in comparison to bulk motion is negligible, the first term in the above equation is removed. Then, we have the following:

$$-\frac{1}{A_r}\frac{\partial}{\partial r}(A_r u_r C_j) + \rho_b\sum_{i=1}^{m} a_i\nu_{ij}r_i - \frac{\mathrm{NOS}}{\pi r R_\theta}\begin{cases}0 & j \neq \mathrm{H_2}\\ J_{\mathrm{H_2}} & j = \mathrm{H_2},\ P_{\mathrm{H_2}} \geq P^s_{\mathrm{H_2}} = 0\\ -J_{\mathrm{H_2}} & j = \mathrm{H_2},\ P^s_{\mathrm{H_2}} > P_{\mathrm{H_2}}\end{cases}\quad \begin{matrix}j = 1, 2, ..., n\\ i = 1, 2, ..., m\end{matrix} \tag{B.16}$$

The first term can be written as follows:

$$-\frac{1}{A_r}\frac{\partial}{\partial r}(A_r u_r C_j) = -\frac{u_r C_j}{A_r}\frac{\partial A_r}{\partial r} - u_r\frac{\partial C_j}{\partial r} - C_j\frac{\partial u_r}{\partial r} = -\frac{u_r C_j}{r} - u_r\frac{\partial C_j}{\partial r} - C_j\frac{\partial u_r}{\partial r} \tag{B.17}$$

By substitution of the new style of the first term,

$$-\frac{u_r C_j}{r} - u_r\frac{\partial C_j}{\partial r} - C_j\frac{\partial u_r}{\partial r} + \rho_b\sum_{i=1}^{m} a_i\nu_{ij}r_i - \frac{\mathrm{NOS}}{\pi r R_\theta}\begin{cases}0 & j \neq \mathrm{H_2}\\ J_{\mathrm{H_2}} & j = \mathrm{H_2},\ P_{\mathrm{H_2}} \geq P^s_{\mathrm{H_2}} = 0\\ -J_{\mathrm{H_2}} & j = \mathrm{H_2},\ P^s_{\mathrm{H_2}} > P_{\mathrm{H_2}}\end{cases}\quad \begin{matrix}j = 1, 2, ..., n\\ i = 1, 2, ..., m\end{matrix} \tag{B.18}$$

And finally, the mass balance becomes as follows:

$$\frac{\partial C_j}{\partial r} = -\frac{C_j}{r} - \frac{C_j}{u_r}\frac{\partial u_r}{\partial r} + \frac{\rho_b}{u_r}\sum_{i=1}^{m} a_i\nu_{ij}r_i - \frac{\mathrm{NOS}}{\pi r R_\theta u_r}\begin{cases}0 & j \neq \mathrm{H_2}\\ J_{\mathrm{H_2}} & j = \mathrm{H_2},\ P_{\mathrm{H_2}} \geq P^s_{\mathrm{H_2}}\\ -J_{\mathrm{H_2}} & j = \mathrm{H_2},\ P^s_{\mathrm{H_2}} > P_{\mathrm{H_2}}\end{cases}\quad \begin{matrix}j = 1, 2, ..., n\\ i = 1, 2, ..., m\end{matrix} \tag{B.19}$$

Energy Balance on the Reaction Side

By considering the reaction side as the system and in the absence of shaft work, the energy balance is as follows:

$$-K_{\mathrm{eff}}A_r\left.\frac{\partial T}{\partial r}\right|_r + K_{\mathrm{eff}}A_r\left.\frac{\partial T}{\partial r}\right|_{r+dr} + \sum_{j=1}^{n} N_j A_r H_j|_r - \sum_{j=1}^{n} N_j A_r H_j|_{r+dr} + 2A_p U(T^s - T) - 2A_p\begin{cases}J_{\mathrm{H_2}}H_{\mathrm{H_2}} & P_{\mathrm{H_2}} \geq P^s_{\mathrm{H_2}}\\ -J_{\mathrm{H_2}}H^s_{\mathrm{H_2}} & P^s_{\mathrm{H_2}} > P_{\mathrm{H_2}}\end{cases} = \frac{\partial(\sum_{j=1}^{n} n_j U_j)}{\partial t} \tag{B.20}$$

By considering the Taylor's extension and dividing the energy balance by A_r dr, we have

$$\frac{1}{A_r}\frac{\partial}{\partial r}\left(K_{\mathrm{eff}}A_r\frac{\partial T}{\partial r}\right) - \frac{1}{A_r}\frac{\partial(\sum_{j=1}^{n} N_j A_r H_j)}{\partial r} + \frac{2A_p}{A_r\,\mathrm{d}r}U(T^s - T) - \frac{2A_p}{A_r\,\mathrm{d}r}\begin{cases}J_{\mathrm{H_2}}\mathrm{H}_{\mathrm{H_2}} & P_{\mathrm{H_2}} \geq P^s_{\mathrm{H_2}}\\ -J_{\mathrm{H_2}}\mathrm{H}^s_{\mathrm{H_2}} & P^s_{\mathrm{H_2}} > P_{\mathrm{H_2}}\end{cases} = \frac{1}{A_r\,\mathrm{d}r}\sum_{j=1}^{n} n_j\frac{\partial U_j}{\partial t} + \frac{1}{A_r\,\mathrm{d}r}\sum_{j=1}^{n} U_j\frac{\partial n_j}{\partial t} \tag{B.21}$$

Substituting eqs B.10 and B.11 in the above equation, the energy balance becomes

$$\frac{1}{A_r}\frac{\partial}{\partial r}\left(K_{\mathrm{eff}}A_r\frac{\partial T}{\partial r}\right) - \frac{1}{A_r}\sum_{j=1}^{n} H_j\frac{\partial(N_j A_r)}{\partial r} - \sum_{j=1}^{n} N_j\frac{\partial H_j}{\partial r} + \frac{\mathrm{NOS}}{\pi r R_\theta}U(T^s - T) - \frac{\mathrm{NOS}}{\pi r R_\theta}\begin{cases}J_{\mathrm{H_2}}\mathrm{H}_{\mathrm{H_2}} & P_{\mathrm{H_2}} \geq P^s_{\mathrm{H_2}}\\ -J_{\mathrm{H_2}}\mathrm{H}^s_{\mathrm{H_2}} & P^s_{\mathrm{H_2}} > P_{\mathrm{H_2}}\end{cases} = \varepsilon\sum_{j=1}^{n} C_j\frac{\partial U_j}{\partial t} + \varepsilon\sum_{j=1}^{n} U_j\frac{\partial C_j}{\partial t} \tag{B.22}$$

The term $\partial(N_j A_r)/\partial r$ is not known and is replaced from eq B.12:

$$\frac{1}{A_r}\frac{\partial}{\partial r}\left(K_{\mathrm{eff}}A_r\frac{\partial T}{\partial r}\right) + \sum_{j=1}^{n} H_j\left(-\rho_b\sum_{i=1}^{m} a_i\nu_{ij}r_i + \frac{\mathrm{NOS}}{\pi r R_\theta}\begin{cases}0 & j \neq \mathrm{H_2}\\ J_{\mathrm{H_2}} & j = \mathrm{H_2},\ P_{\mathrm{H_2}} \geq P^s_{\mathrm{H_2}}\\ -J_{\mathrm{H_2}} & j = \mathrm{H_2},\ P^s_{\mathrm{H_2}} > P_{\mathrm{H_2}}\end{cases} + \varepsilon\frac{\partial C_j}{\partial t} - \sum_{j=1}^{n} N_j\frac{\partial H_j}{\partial r} + \frac{\mathrm{NOS}}{\pi r R_\theta}U(T^s - T) - \frac{\mathrm{NOS}}{\pi r R_\theta}\begin{cases}J_{\mathrm{H_2}}H_{\mathrm{H_2}} & P_{\mathrm{H_2}} \geq P^s_{\mathrm{H_2}}\\ -J_{\mathrm{H_2}}H^s_{\mathrm{H_2}} & P^s_{\mathrm{H_2}} > P_{\mathrm{H_2}}\end{cases} = \varepsilon\sum_{j=1}^{n} C_j\frac{\partial U_j}{\partial t} + \varepsilon\sum_{j=1}^{n} U_j\frac{\partial C_j}{\partial t} \tag{B.23}$$

hence:

dx.doi.org/10.1021/ef302057k | Energy Fuels 2013, 27, 4048−4070

$$\frac{1}{A_r}\frac{\partial}{\partial r}\left(K_{\text{eff}}A_r\frac{\partial T}{\partial r}\right)-\sum_{j=1}^{n}H_j(\rho_b\sum_{i=1}^{m}a_i\nu_{ij}r_i)+\sum_{j=1}^{n}\left(H_j\frac{\text{NOS}}{\pi rR_\theta}\begin{cases}0 & j\neq \text{H}_2\\ J_{\text{H}_2} & j=\text{H}_2,\ P_{\text{H}_2}\geq P^{\text{s}}_{\text{H}_2}\\ -J_{\text{H}_2} & j=\text{H}_2,\ P^{\text{s}}_{\text{H}_2}>P_{\text{H}_2}\end{cases}\right)+\sum_{j=1}^{n}H_j\varepsilon\frac{\partial C_j}{\partial t}-\sum_{j=1}^{n}N_j\frac{\partial H_j}{\partial r}+\frac{\text{NOS}}{\pi rR_\theta}U(T^{\text{s}}-T)-\frac{\text{NOS}}{\pi rR_\theta}\begin{cases}J_{\text{H}_2}H_{\text{H}_2} & P_{\text{H}_2}\geq P^{\text{s}}_{\text{H}_2}\\ -J_{\text{H}_2}H^{\text{s}}_{\text{H}_2} & P^{\text{s}}_{\text{H}_2}>P_{\text{H}_2}\end{cases}=\varepsilon\sum_{j=1}^{n}C_j\frac{\partial U_j}{\partial t}+\varepsilon\sum_{j=1}^{n}U_j\frac{\partial C_j}{\partial t}\tag{B.24}$$

The third term in the above equation can be reduced to the following:

$$\sum_{j=1}^{n}H_j\left(\frac{\text{NOS}}{\pi rR_\theta}\begin{cases}0 & j\neq \text{H}_2\\ J_{\text{H}_2} & j=\text{H}_2,\ P_{\text{H}_2}\geq P^{\text{s}}_{\text{H}_2}\\ -J_{\text{H}_2} & j=\text{H}_2,\ P^{\text{s}}_{\text{H}_2}>P_{\text{H}_2}\end{cases}\right)=\frac{\text{NOS}}{\pi rR_\theta}\sum_{j=1}^{n}\left(\begin{cases}0H_j & j\neq \text{H}_2\\ J_{\text{H}_2}\text{H}_{\text{H}_2} & j=\text{H}_2,\ P_{\text{H}_2}\geq P^{\text{s}}_{\text{H}_2}\\ -J_{\text{H}_2}\text{H}_{\text{H}_2} & j=\text{H}_2,\ P^{\text{s}}_{\text{H}_2}>P_{\text{H}_2}\end{cases}\right)=\frac{\text{NOS}}{\pi rR_\theta}\begin{cases}J_{\text{H}_2}H_{\text{H}_2} & P_{\text{H}_2}\geq P^{\text{s}}_{\text{H}_2}\\ -J_{\text{H}_2}\text{H}_{\text{H}_2} & P^{\text{s}}_{\text{H}_2}>P_{\text{H}_2}\end{cases}\tag{B.25}$$

Now we have

$$\frac{1}{A_r}\frac{\partial}{\partial r}\left(K_{\text{eff}}A_r\frac{\partial T}{\partial r}\right)-\rho_b(\sum_{i=1}^{m}\sum_{j=1}^{n}(H_j\nu_{ij})a_ir_i)-\sum_{j=1}^{n}N_j\frac{\partial H_j}{\partial r}+\frac{\text{NOS}}{\pi rR_\theta}U(T^{\text{s}}-T)+\frac{\text{NOS}}{\pi rR_\theta}\begin{cases}J_{\text{H}_2}H_{\text{H}_2} & P_{\text{H}_2}\geq P^{\text{s}}_{\text{H}_2}\\ -J_{\text{H}_2}H_{\text{H}_2} & P^{\text{s}}_{\text{H}_2}>P_{\text{H}_2}\end{cases}-\frac{\text{NOS}}{\pi rR_\theta}\begin{cases}J_{\text{H}_2}H_{\text{H}_2} & P_{\text{H}_2}\geq P^{\text{s}}_{\text{H}_2}\\ -J_{\text{H}_2}H^{\text{s}}_{\text{H}_2} & P^{\text{s}}_{\text{H}_2}>P_{\text{H}_2}\end{cases}=\varepsilon\sum_{j=1}^{n}C_j\frac{\partial U_j}{\partial t}+\varepsilon\sum_{j=1}^{n}(U_j-H_j)\frac{\partial C_j}{\partial t}\tag{B.26}$$

The following definitions are used to simplify the recent equation:

$$\Delta H_i=\sum_{j=1}^{n}(\nu_{ij}H_j)\tag{B.27}$$

$$\frac{\partial H_j}{\partial r}=\frac{\partial H_j}{\partial T}\frac{\partial T}{\partial r}=C_{P_j}\frac{\partial T}{\partial r}\tag{B.28}$$

$$\sum_{j=1}^{n}N_j\frac{\partial H_j}{\partial r}=\sum_{j=1}^{n}\left((J_j+C_ju_r)C_{P_j}\frac{\partial T}{\partial r}\right)=\frac{\partial T}{\partial r}\sum_{j=1}^{n}((J_j+C_ju_r)C_{P_j})\simeq u_r(\sum_{j=1}^{n}C_jC_{P_j})\frac{\partial T}{\partial r}\tag{B.29}$$

$$\left(\sum_{j=1}^{n}C_jC_{P_j}\right)=C_{\text{T}}\left(\sum_{j=1}^{n}\left(\frac{C_j}{C_{\text{T}}}\right)C_{P_j}\right)=C_{\text{T}}\sum_{j=1}^{n}y_jC_{P_j}=C_{\text{T}}C_P\tag{B.30}$$

$$(U_j-H_j)=-P\nu_j=-RT\tag{B.31}$$

$$\sum_{j=1}^{n}(U_j-H_j)\frac{\partial C_j}{\partial t}=-RT\sum_{j=1}^{n}\frac{\partial C_j}{\partial t}=-RT\frac{\partial C_{\text{T}}}{\partial t}\tag{B.32}$$

$$\frac{\partial U_j}{\partial t}=\frac{\partial U_j}{\partial T}\frac{\partial T}{\partial t}=C_{V_j}\frac{\partial T}{\partial t}\tag{B.33}$$

$$C_{V_j}=C_{P_j}-R\tag{B.34}$$

$$C_V=C_P-R\tag{B.35}$$

Additionally

$$\sum_{j=1}^{n}C_j\frac{\partial U_j}{\partial t}=\sum_{j=1}^{n}C_jC_{V_j}\frac{\partial T}{\partial t}=\frac{\partial T}{\partial t}\sum_{j=1}^{n}C_jC_{V_j}=(\sum_{j=1}^{n}C_jC_{V_j})\frac{\partial T}{\partial t}\tag{B.36}$$

$$(\sum_{j=1}^{n}C_jC_{V_j})=C_{\text{T}}\left(\sum_{j=1}^{n}\left(\frac{C_j}{C_{\text{T}}}\right)C_{V_j}\right)=C_{\text{T}}\sum_{j=1}^{n}y_jC_{V_j}=C_{\text{T}}C_V\tag{B.37}$$

where C_V and C_P are the average heat capacities of mixture at constant volume and pressure, respectively. Accordingly, on the basis of the above definition:

$$\frac{1}{A_r}\frac{\partial}{\partial r}\left(K_{\text{eff}}A_r\frac{\partial T}{\partial r}\right)-\rho_{\text{b}}(\sum_{i=1}^{m}\Delta H_ia_ir_{\text{i}})-u_rC_{\text{T}}C_P\frac{\partial T}{\partial r}+\frac{\text{NOS}}{\pi rR_\theta}U(T^{\text{s}}-T)+\frac{\text{NOS}}{\pi rR_\theta}\begin{cases}J_{\text{H}_2}(H_{\text{H}_2}-H_{\text{H}_2}) & P_{\text{H}_2}\geq P^{\text{s}}_{\text{H}_2}\\ J_{\text{H}_2}(-H_{\text{H}_2}+H^{\text{s}}_{\text{H}_2}) & P^{\text{s}}_{\text{H}_2}>P_{\text{H}_2}\end{cases}=\varepsilon C_{\text{T}}C_V\frac{\partial T}{\partial t}-\varepsilon RT\frac{\partial C_{\text{T}}}{\partial t}\tag{B.38}$$

and then,

dx.doi.org/10.1021/ef302057k | Energy Fuels 2013, 27, 4048−4070

$$\frac{1}{A_r}\frac{\partial}{\partial r}\left(K_{\text{eff}}A_r\frac{\partial T}{\partial r}\right)-\rho_b\left(\sum_{i=1}^{m}\Delta H_i a_i r_i\right)-u_r C_T C_P\frac{\partial T}{\partial r}+\frac{\text{NOS}}{\pi r R_\theta}U(T^s-T)+\frac{\text{NOS}}{\pi r R_\theta}\begin{cases}J_{H_2}(H_{H_2}-H_{H_2}) & P_{H_2}\geq P^s_{H_2}\\ J_{H_2}(-H_{H_2}+H^s_{H_2}) & P^s_{H_2}>P_{H_2}\end{cases}+\varepsilon RT\frac{\partial C_T}{\partial t}=\varepsilon C_T C_V\frac{\partial T}{\partial t} \tag{B.39}$$

Now, we define γ_{H_2} and then

$$\frac{1}{A_r}\frac{\partial}{\partial r}\left(K_{\text{eff}}A_r\frac{\partial T}{\partial r}\right)-\rho_b\left(\sum_{i=1}^{m}\Delta H_i a_i r_i\right)-u_r C_T C_P\frac{\partial T}{\partial r}+\frac{\text{NOS}}{\pi r R_\theta}U(T^s-T)+\frac{\text{NOS}}{\pi r R_\theta}J_{H_2}\{\gamma_{H_2}-H_{H_2}\}+\varepsilon RT\frac{\partial C_T}{\partial t}=\varepsilon C_T C_V\frac{\partial T}{\partial t} \tag{B.40}$$

and in the final analysis, γ_{H2} is defined as shown below:[48,49]

$$\gamma_{H_2}=\begin{cases}H_{H_2} & P_{H_2}\geq P^s_{H_2}\\ H^s_{H_2} & P_{H_2}<P^s_{H_2}\end{cases} \tag{B.41}$$

By neglecting conductive heat transfer in comparison to convective heat transfer and heat of reaction,

$$-u_r C_T C_P\frac{\partial T}{\partial r}-\rho_b\sum_{i=1}^{m}(\Delta H_i a_i r_i)+\frac{\text{NOS}}{\pi r R_\theta}U(T^s-T)+\frac{\text{NOS}}{\pi r R_\theta}\begin{cases}J_{H_2}(H_{H_2}-H_{H_2}) & P_{H_2}\geq P^s_{H_2}\\ J_{H_2}(-H_{H_2}+H^s_{H_2}) & P^s_{H_2}>P_{H_2}\end{cases}=0 \tag{B.42}$$

and finally,

$$\frac{\partial T}{\partial r}=-\frac{\rho_b}{u_r C_T C_P}\sum_{i=1}^{m}(\Delta H_i a_i r_i)+\frac{\text{NOS}}{\pi r R_\theta u_r C_T C_P}U(T^s-T)+\frac{\text{NOS}}{\pi r R_\theta u_r C_T C_P}\begin{cases}J_{H_2}(H_{H_2}-H_{H_2}) & P_{H_2}\geq P^s_{H_2}\\ J_{H_2}(-H_{H_2}+H^s_{H_2}) & P^s_{H_2}>P_{H_2}\end{cases} \tag{B.43}$$

Velocity Distribution on the Reaction Side

To obtain a velocity distribution equation, the mass balance equation is used.

$$\frac{\partial C_j}{\partial r}=-\frac{C_j}{r}-\frac{C_j}{u_r}\frac{\partial u_r}{\partial r}+\frac{\rho_b}{u_r}\sum_{i=1}^{m}a_i\nu_{ij}r_i-\frac{\text{NOS}}{\pi r R_\theta u_r}\begin{cases}0 & j\neq H_2\\ J_{H_2} & j=H_2,\ P_{H_2}\geq P^s_{H_2}\\ -J_{H_2} & j=H_2,\ P^s_{H_2}>P_{H_2}\end{cases}\quad\begin{matrix}j=1,2,\ldots,n\\ i=1,2,\ldots,m\end{matrix} \tag{B.44}$$

Then, by integrating the above equation

$$\sum_{j=1}^{n}\frac{\partial C_j}{\partial r}=-\sum_{j=1}^{n}\frac{C_j}{r}-\frac{1}{u_r}\frac{\partial u_r}{\partial r}\sum_{j=1}^{n}C_j+\frac{\rho_b}{u_r}\sum_{j=1}^{n}\sum_{i=1}^{m}a_i\nu_{ij}r_i-\sum_{j=1}^{n}\frac{\text{NOS}}{\pi r R_\theta u_r}\begin{cases}0 & j\neq H_2\\ J_{H_2} & j=H_2,\ P_{H_2}\geq P^s_{H_2}\\ -J_{H_2} & j=H_2,\ P^s_{H_2}>P_{H_2}\end{cases} \tag{B.45}$$

By considering $\sum C_j = C_T$, the velocity equation becomes

$$\frac{\partial C_T}{\partial r}=-\frac{C_T}{r}-\frac{C_T}{u_r}\frac{\partial u_r}{\partial r}+\frac{\rho_b}{u_r}\sum_{j=1}^{n}\sum_{i=1}^{m}a_i\nu_{ij}r_i-\frac{\text{NOS}}{\pi r R_\theta u_r}\begin{cases}J_{H_2} & P_{H_2}\geq P^s_{H_2}\\ -J_{H_2} & P^s_{H_2}>P_{H_2}\end{cases} \tag{B.46}$$

The above equation is multiplied by u_r/C_T

$$\frac{u_r}{C_T}\frac{\partial C_T}{\partial r}=-\frac{u_r}{r}-\frac{\partial u_r}{\partial r}+\frac{\rho_b}{C_T}\sum_{j=1}^{n}\sum_{i=1}^{m}a_i\nu_{ij}r_i-\frac{\text{NOS}}{\pi r R_\theta C_T}\begin{cases}J_{H_2} & P_{H_2}\geq P^s_{H_2}\\ -J_{H_2} & P^s_{H_2}>P_{H_2}\end{cases} \tag{B.47}$$

Eventually, the velocity distribution equation is as follows:

$$\frac{\partial u_r}{\partial r}=-\frac{u_r}{r}-\frac{u_r}{C_T}\frac{\partial C_T}{\partial r}+\frac{\rho_b}{C_T}\sum_{j=1}^{n}\sum_{i=1}^{m}a_i\nu_{ij}r_i-\frac{\text{NOS}}{\pi r R_\theta C_T}\begin{cases}J_{H_2} & P_{H_2}\geq P^s_{H_2}\\ -J_{H_2} & P^s_{H_2}>P_{H_2}\end{cases} \tag{B.48}$$

To find $\partial C_T/\partial r$ in this equation, we use the ideal gas law

$$C_T=\frac{P}{RT} \tag{B.49}$$

Then by doing the following algebraic operations on the above relations, we have

$$\frac{\partial C_T}{\partial r}=\frac{1}{RT}\frac{\partial P}{\partial r}-\frac{P}{RT^2}\frac{\partial T}{\partial r} \tag{B.50}$$

Mass and Energy Balances and Velocity Distribution on the Sweep Gas Side

With same procedure, for the sweep gas side, we have the following:

Mass Balance.

$$\frac{\partial C^s_j}{\partial r}=-\frac{C^s_j}{r}-\frac{C^s_j}{u^s_r}\frac{\partial u^s_r}{\partial r}+\frac{\text{NOS}}{\pi r(1-R_\theta)u^s_r}\begin{cases}0 & j\neq H_2\\ J_{H_2} & j=H_2,\ P_{H_2}\geq P^s_{H_2}\\ -J_{H_2} & j=H_2,\ P^s_{H_2}>P_{H_2}\end{cases}\quad j=1,2,\ldots,n' \tag{B.51}$$

Where n' is the number of components in the sweep gas side.

dx.doi.org/10.1021/ef302057k | Energy Fuels 2013, 27, 4048−4070

Energy Balance.

$$\frac{\partial T^s}{\partial r} = \frac{\mathrm{NOS}}{\pi r(1-R_\theta)u_r^s C_T^s C_P} U(T - T^s) - \frac{\mathrm{NOS}}{\pi r(1-R_\theta)u_r^s C_T^s C_P}\begin{cases} J_{H_2}(H_{H_2} - H_{H_2}) & P_{H_2} \geq P_{H_2}^s \\ J_{H_2}(-H_{H_2} + H_{H_2}^s) & P_{H_2}^s > P_{H_2} \end{cases} \tag{B.52}$$

Velocity Distribution.

$$\frac{\partial u_r^s}{\partial r} = -\frac{u_r^s}{r} - \frac{u_r^s}{C_T^s}\frac{\partial C_T^s}{\partial r} + \frac{\mathrm{NOS}}{\pi r(1-R_\theta)C_T^s}\begin{cases} J_{H_2} & P_{H_2} \geq P_{H_2}^s \\ -J_{H_2} & P_{H_2}^s > P_{H_2} \end{cases} \tag{B.53}$$

Collector Mass and Energy Balance

The mass balance in the collector can be written as follows:

$$F_j|_z - F_j|_{z+dz} + F_{je} = 0 \quad j = 1, 2, ..., n \tag{B.54}$$

Where F_j is molar flow rate of component j in the Z direction and F_{je} is output molar flow rate of component j from reaction side that enters to the collector.

$$F_{je} = C_{je}u_{re}A_{re} = C_{je}u_{re}\frac{2\pi R_i}{\mathrm{NOS}}\,\mathrm{d}zR_\theta \quad j = 1, 2, ..., n \tag{B.55}$$

where, C_{je} and u_{re} are the concentrations of component j and the radial velocity in inner radius of reactor

By considering the Taylor's extension, the mass balance equation is changed to the following:

$$\frac{\partial F_j}{\partial z} = \frac{2\pi R_i}{\mathrm{NOS}}u_{re}C_{je}R_\theta \quad j = 1, 2, ..., n \tag{B.56}$$

Then, to calculate total molar flow rate (F_T), the summation of the recent equation for all pseudocomponents on the reaction side is considered:

$$\sum_{j=1}^{n}\frac{\partial F_j}{\partial z} = \sum_{j=1}^{n}\left(\frac{2\pi R_i}{\mathrm{NOS}}u_{re}C_{je}R_\theta\right) \tag{B.57}$$

$$\sum_{j=1}^{n}\frac{\partial F_j}{\partial z} = \frac{2\pi R_i}{NOS}u_{re}R_\theta\sum_{j=1}^{n}(C_{je}) \tag{B.58}$$

Finally, because $\sum C_{je} = C_{Te}$, we have

$$\frac{\partial F_T}{\partial z} = \frac{2\pi R_i}{\mathrm{NOS}}u_{re}R_\theta C_{Te} \tag{B.59}$$

Where

$$F_T = \sum_{j=1}^{32}F_j \tag{B.60}$$

The energy balance in the collector can be written as follows:

$$F_T C_P T|_z - F_T C_P T|_{z+dz} + \sum_{j=1}^{n}F_{je}C_{p_{je}}(T_e - T) = 0 \tag{B.61}$$

where

$$C_p = \frac{\sum_{j=1}^{m}F_j C_{p_j}}{F_T} \tag{B.62}$$

Equation B.55 is substituted in energy balance and the below equation is obtained,

$$F_T C_P T|_z - F_T C_P T|_{z+dz} + \sum_{j=1}^{n}C_{je}u_{re}\frac{2\pi R_i}{\mathrm{NOS}}\,\mathrm{d}z\,R_\theta C_{p_{je}}(T_e - T) = 0 \tag{B.63}$$

By considering the Taylor's extension, the energy balance equation is changed to

$$\frac{\partial(F_T C_P T)}{\partial z} = \sum_{j=1}^{n}C_{je}u_{re}\frac{2\pi R_i}{\mathrm{NOS}}R_\theta C_{p_{je}}(T_e - T) \tag{B.64}$$

as we know

$$\sum_{j=1}^{n}(C_{je}C_{p_{je}}) = C_{Te}\sum_{j=1}^{n}\left(\left(\frac{C_{je}}{C_{Te}}\right)C_{p_{je}}\right) = C_{Te}\sum_{j=1}^{n}(y_{je}C_{p_{je}}) = C_{Te}C_{p_e} \tag{B.65}$$

Then

$$\frac{\partial(F_T C_P T)}{\partial z} = C_{Te}u_{re}\frac{2\pi R_i}{\mathrm{NOS}}R_\theta C_{p_e}(T_e - T) \tag{B.66}$$

$$C_P T\frac{\partial(F_T)}{\partial z} + F_T C_P\frac{\partial(T)}{\partial z} + F_T T\frac{\partial(C_P)}{\partial z} = \frac{2\pi R_i}{\mathrm{NOS}}C_{Te}u_{re}R_\theta C_{p_e}(T_e - T) \tag{B.67}$$

$$\frac{1}{T}\frac{\partial T}{\partial z} + \frac{1}{C_P}\frac{\partial C_P}{\partial z} + \frac{1}{F_T}\frac{\partial F_T}{\partial z} = \frac{1}{F_T C_P T}\frac{2\pi R_i}{\mathrm{NOS}}C_{Te}u_{re}R_\theta C_{p_e}(T_e - T) \tag{B.68}$$

$$\frac{\partial T}{\partial z} = \frac{1}{F_T C_P}\frac{2\pi R_i}{\mathrm{NOS}}C_{Te}u_{re}R_\theta C_{p_e}(T_e - T) - \frac{T}{F_T}\left(\frac{2\pi R_i}{\mathrm{NOS}}u_{re}R_\theta C_{Te}\right) - \frac{T}{C_P}\frac{\partial C_P}{\partial z} \tag{B.69}$$

With same procedure for sweep gas section in the collector, the mass and energy balances are defined as follows:

$$\frac{\partial F_j^s}{\partial z} = \frac{2\pi R_i}{\mathrm{NOS}}u_{re}^s C_{je}^s(1 - R_\theta) \quad j = 1, 2, ..., n' \tag{B.70}$$

$$\frac{\partial T^s}{\partial z} = \frac{C_{Te}^s u_{re}^s}{F_T^s C_P}\frac{2\pi R_i}{\mathrm{NOS}}(1 - R_\theta)C_{p_e}(T_e^s - T^s) - \frac{T^s}{F_T^s}\left(\frac{2\pi R_i}{\mathrm{NOS}}u_{re}^s(1 - R_\theta)C_{Te}^s\right) - \frac{T^s}{C_P}\frac{\partial C_P}{\partial z} \tag{B.71}$$

Nomenclature

a_i = catalyst activity
a_A = acidic function activity
a_{C_A} = acidic function activity for coke formation
a_{C_M} = metallic function activity for coke formation
a_M = metallic function activity
A_r = Cross-sectional area of reactor in radial direction, m^2
A_p = surface area of membrane, m^2
C = concentration, $kmol/m^3$
C_{ACP} = alkyl-cyclopentane concentration, $kmol/m^3$
C_{C_A} = coke weight fraction on acidic function of catalyst, kg/kg_{cat}

dx.doi.org/10.1021/ef302057k | *Energy Fuels* 2013, 27, 4048−4070

C_{C_M} = coke weight fraction on metallic function of catalyst, kg/kg_{cat}
C_{j0} = inlet concentration of component j, $kmol/m^3$
C_P = specific heat capacity at constant pressure, kJ/(kmol K)
C_V = specific heat capacity at constant volume, kJ/(kmol K)
C_T = total concentration, $kmol/m^3$
d_p = particle diameter, m
D_e = effective diffusivity, m^2/s
E_c = coke formation activation energy, J/mol
F = molar flow rate, kmol/h
F_j = molar flow rate of component j, kmol/h
F_T = total molar flow rate to the reactor, kmol/h
J_{H_2} = hydrogen permeation rate, $kmol/(m^2\ h)$
H = enthalpy, J/mol
H_j = Enthalpy of component j, J/mol
k = thermal conductivity, W/(m K)
K_{C_A} = constant of deactivation equation for acidic function, $(kg\ kPa^{n_1}\ m^{1.5})/(kg\ kmol^{1.5})$
K_{C_M} = constant of deactivation equation for metallic function, $(kg\ kPa^{n}{}_1\ m^{1.5})/(kg\ kmol^{1.5})$
k_{eff} = effective thermal conductivity, W/(m K)
k_{in} = reaction rate constant for reaction (in)
K_{in} = equilibrium constant for reaction (in)
L = length of reactor, m
m = number of reactions
M_j = molecular weight of component j, kg/kmol
M = mean molecular weight in the flow, kg/kmol
n = number of components
n_1 = constant of deactivation equation
n_2 = constant of deactivation equation
n_A = acidic function activity power number
n_{C_A} = acidic function activity power number
n_M = metallic function activity power number
n_{C_M} = metallic function activity power number
N_j = molar flux of component j, $kmol/(m^2\ h)$
P = total pressure, kPa
P_{An} = partial pressure of n carbon aromatic, kPa
P_{ACHn} = partial pressure of n carbon alkyl-cyclohexane, kPa
P_{ACPn} = partial pressure of n carbon alkyl-cyclopentane, kPa
P_{H2} = partial pressure of hydrogen, kPa
P_{IPn} = partial pressure of n carbon iso-paraffin with, kPa
P_{NPn} = partial pressure of n carbon normal-paraffin, kPa
r = radius, m
r_i = rate of ith reaction, $kmol/(kg_{cat}\ h)$
r_{in} = rate of inth reaction, $kmol/(kg_{cat}\ h)$
r_C^0 = rate of coke formation on fresh catalyst, $kg/(kg_{cat}\ h)$
r_{C_A} = rate of coke formation on acidic function of catalyst, $kg/(kg_{cat}\ h)$
r_{C_M} = rate of coke formation on metallic function of catalyst, $kg/(kg_{cat}\ h)$
R = gas constant, J/(mol K)
R_i = inner diameter, m
R_o = outer diameter, m
S_a = specific surface, m^2/g
T = temperature, K
U = overall heat transfer coefficient, $W/(m^2\ K)$
U_j = internal energy of component j, J/mol
u_r = radial velocity, m/s
y_j = mole fraction of component j

Greek Letters

ε = void fraction of catalyst bed
μ = viscosity, kg/(m s)
v_{ij} = stoichiometric coefficient of component j in reaction i
ρ_b = reactor bulk density, kg/m^3
ϕ_s = sphericity
θ_1 = reaction side angle
θ_2 = sweep side angle
δ_{H_2} = membrane thickness, m
ΔH = heat of reaction, kJ/mol
Δz = control volume length, m
Δr = control volume thickness in radial direction, m
α_A = constant of deactivation, $m^3/kmol$
α_{C_A} = constant of deactivation, $m^3/kmol$
α_{C_M} = constant of deactivation, $m^3/kmol$
π = Pi
α_M = constant of deactivation, $m^3/kmol$

Superscript

s = sweep side

Subscript

e = exit condition
i = numerator for reaction
j = numerator for component
n = number of carbon atoms
T = total

Abbreviations

A = aromatics
ACH = alkyl-cyclohexane
ACP = alkyl-cyclopentane
CCR = continuous catalyst regenerative
CR = conventional reactor
FBP = final boiling point
HC = hydrocarbon
IBP = initial boiling point, °C
IP = iso-paraffin
LOD = length over diameter
NOS = number of subsections
NP = normal-paraffin
MR = membrane reactor
Pd−Ag = palladium−silver
Pt = platinum
Sn = tin

AUTHOR INFORMATION

Corresponding Author

*Tel.: +98 711 2303071. Fax: +98 711 6287294. E-mail: rahimpor@shirazu.ac.ir; mrahimpour@ucdavis.edu.

Notes

The authors declare no competing financial interest.

REFERENCES

(1) Antos, G. J.; Aitani, A. M. *Catalytic Naphtha Reforming*, 2nd ed.; Marcel Dekker Inc.: New York, 1995.
(2) Aitani, A. M. *Encyclopedia of Chemical Processing*; Taylor & Francis: London, 2005.
(3) Hou, W.; Hu, Y.; Su H.; Chu, J. *Proceedings of the 5th World Congress on Intelligent Control and Automation*, Hangzhou, P.R. China, June 15−19, 2004.
(4) Smith, R. B. *Chem. Eng. Prog.* **1959**, *55*, 76−80.
(5) Krane, H. G.; Groh, A. B.; Schulman, B. L.; Sinfelt, J. H. *Proc. World Pet. Congr.* **1960**, *3*, 39−53.
(6) Kmak, W. S. A Kinetic Simulation Model of the Powerforming Process. *AIChE National Meeting*, Houston, TX, 1972.
(7) Ramage, M. P.; Graziani, K. P.; Krambeck, F. J. *Chem. Eng. Sci.* **1980**, *35*, 41−48.
(8) Jenkins, J. H.; Stephens, T. W. *Hydro. Process* **1980**, *11*, 163−167.

(9) Wolff, A.; Kramarz, J. *Chem. Technol. Fuels Oils* **1979**, *15*, 870−877.
(10) Juarez, J. A.; Macias, E. V. *Energy Fuels* **2000**, *14*, 1032−1037.
(11) Sotelo-Boyas, R.; Froment, G. F. *Ind. Eng. Chem. Res.* **2009**, *48*, 1107−1119.
(12) Hu, Y.; Su, H.; Chu, J. *Proceedings of the 42nd IEEE Conference on Decision and Control*, Maui, Hawaii, December 2003.
(13) Hu, S.; Zhu, X. X. *Chem. Eng. Commun.* **2004**, *191*, 500−512.
(14) Hongjun, Z.; Mingliang, S.; Huixin, N.; Zeji, L.; Hongbo, J. *Petr. Sci. Technol.* **2010**, *28*, 667−676.
(15) Otal, L. M. R.; Garcia, T. V.; Rubio, M. S. *Stud. Surf. Sci. Catal.* **1997**, *111*, 319−325.
(16) Gonzalez-Marcos, M. P.; Inarra, B.; Guil, J. M.; Gutierrez-Ortiz, M. A. *Catal. Today* **2005**, *107−108*, 685−692.
(17) Pieck, C. L.; Sad, M. R.; Parera, J. M. *J. Chem. Technol. Biotechnol.* **1996**, *67*, 61−66.
(18) Ren, X. H.; Bertmer, M.; Stapf, S.; Demco, D. E.; Blümich, B.; Kern, C.; Jess, A. *Appl. Catal., A* **2002**, *228*, 39−52.
(19) Carvalho, L. S.; Pieck, C. L.; Rangel, M. C.; Figoli, N. S.; Grau, J. M.; Reyes, P.; Parera, J. M. *Appl. Catal. A* **2004**, *269*, 91−103.
(20) Borgna, A.; Garetto, T. F.; Monzon, M.; Apesteguia, C. R. *J. Catal.* **1994**, *146*, 69−81.
(21) Viswanadham, N.; Kamble, R.; Sharma, A.; Kumar, M.; Saxena, A. K. *J. Mol. Catal. A: Chem.* **2008**, *282*, 74−79.
(22) Martin, N.; Viniegra, M.; Zarate, R.; Espinosa, G.; Batina, N. *Catal. Today* **2005**, *107−108*, 719−725.
(23) Taskar, U.; Riggs, J. B. *AIChE J.* **1997**, *43*, 740−753.
(24) Juarez, J. A.; Macias, E. V.; Garcia, L. D.; Arredondo, E. G. *Energy Fuels* **2001**, *15*, 887−893.
(25) Li, J.; Tan, Y.; Liao, L. *Conference on control application*, 2005.
(26) Hou, W.; Su, H.; Hu, Y.; Chu, J. *Chin. J. Chem. Eng.* **2006**, *14*, 584−591.
(27) Khosravanipour Mostafazadeh, A.; Rahimpour, M. R. *Chem. Eng. Process* **2009**, *48*, 683−694.
(28) Stijepovic, M. Z.; Linke, P.; Kijevcanin, M. *Energy Fuels* **2010**, *24*, 1908−1916.
(29) Mahdavian, M.; Fatemi, S.; Fazeli, A. *Int. J. Chem. Reactor Eng.* **2010**, *8* (1), XXX.
(30) Lee, J. W.; Ko, Y. C.; Jung, Y. K.; Lee, K. S. *Comput. Chem. Eng.* **1997**, 1105−1110.
(31) Abdel Gawad, A. K.; Ashour, H.; Zakzouk, E. E. In *Proceedings of 2003 IEEE Conference on Control Applications*, Istanbul, June 23−25, 2003.
(32) Rafiei, R.; Amiri, S.; Mirvakili, A.; Iranshahi, D.; Rahimpour, M. R. *Energy Fuels* **2012**, *26*, 5858−5871.
(33) Nam, S. E.; Lee, K. H. *J. Membr. Sci.* **2001**, *192*, 177−185.
(34) Okazaki, J.; Tanaka, D. A. P.; Tanco, M. A. L.; Wakui, Y.; Mizukami, F.; Suzuki, T. M. *J. Membr. Sci.* **2006**, *282*, 370−374.
(35) Dittmeyer, R.; Höllein, V.; Daub, K. *J. Mol. Catal. A: Chem.* **2001**, *173*, 135−184.
(36) Baker, R. W. *Ind. Eng. Chem. Res.* **2002**, *41*, 1393−1411.
(37) Rahimpour, M. R.; Iranshahi, D.; Pourazadi, E.; Paymooni, K.; Bahmanpour, A. M. *AIChE J.* **2011**, *57*, 3182−3198.
(38) Hodoshima, S.; Shono, A.; Saito, Y. *Energy Fuels* **2008**, *2*, 2559−2569.
(39) Liao, Z.; Wang, J.; Yang, Y.; Rong, G. *J. Clean Prod.* **2010**, *18*, 233−241.
(40) Hallale, N.; Liu, F. *Adv. Environ. Sci.* **2001**, *6*, 81−98.
(41) Aitani, A. M.; Ali, S. A. *Erdoel Kohle, Erdgas, Petr.* **1995**, *48*, 19−24.
(42) Padmavathi, G.; Chaudhuri, K. K. *Can. J. Chem. Eng.* **1997**, *75*, 930−937.
(43) Liu, K.; Fung, S. C.; Ho, T. C.; Rumschitzki, D. S. *J. Catal.* **2002**, *206*, 188−201.
(44) Liu, K.; Fung, S. C.; Ho, T. C.; Rumschitzki, D. S. *Ind. Eng. Chem. Res.* **1997**, *36*, 3264−3274.
(45) Tailleur, R. G.; Davila, Y. *Energy Fuels.* **2008**, *22*, 2892−2901.
(46) Brinkmann, T.; Perera, S. P.; Thomas, W. J. *Chem. Eng. Sci.* **2001**, *56*, 2047.
(47) Alhumaizi, K. *Comput. Chem. Eng.* **2004**, *28*, 1759−1769.
(48) Fogler, H. S. *Elements of Chemical Reaction Engineering*, 2nd ed.; Prentice-Hall Englewood Cliffs: New York, 1992.
(49) Barbieri, G.; Marigliano, G.; Golemme, G.; Drioli, E. *Chem. Eng. J.* **2002**, *85*, 53−59.